JGR Atmospheres

RESEARCH ARTICLE
10.1029/2021JD035236

Key Points:

- With the increase in pollution and the decrease in planetary boundary layer height, more aerosols are accumulated at the lower height
- The aerosol extinction coefficients decrease significantly with height below 2 km, and aerosol scattering ability is strong in 0~2 km
- The regular fine particles with lower particulate depolarization ratio (PDR) (79% of the PDR is <0.2), lower lower color ratio (CR) (64% of the CR is <0.75) are dominant in 0~2 km

Correspondence to:
Y. Han,
hany66@mail.sysu.edu.cn

Citation:
Zhang, Y., Wei, F., Luo, H., Su, Y., Feng, Y., Huang, Y., et al. (2021). Aerosol physical-optical properties and PBLH under different air pollution levels from ground Lidar and satellite observations over Shouxian area, China. *Journal of Geophysical Research: Atmospheres*, *126*, e2021JD035236. https://doi.org/10.1029/2021JD035236

Received 11 MAY 2021
Accepted 10 DEC 2021

Aerosol Physical-Optical Properties and PBLH Under Different Air Pollution Levels From Ground Lidar and Satellite Observations Over Shouxian Area, China

Yuan Zhang[1], Fan Wei[2], Hao Luo[1], Yueyuan Su[1], Yan Feng[3,4], Yong Huang[3,4], Jun Yang[5], Yonghua Wu[6], and Yong Han[1,7,8]

[1]Advanced Science & Technology of Atmospheric Physics Group (ASAG), School of Atmospheric Sciences, Sun Yat-sen University, Zhuhai, China, [2]Anhui Engineering and Technology Research Center of Smart City, School of Environment and Energy Engineering, Anhui JIANZHU University, Anhui, China, [3]Key Laboratory of Atmospheric Science and Satellite Remote Sensing Anhui Province, Anhui Institute of Meteorological Sciences, Hefei, China, [4]Huaihe River Basin Typical Farm Eco-meteorological Experiment Field of CMA, Shouxian National Climatology Observatory, Shouxian, China, [5]State Key Laboratory of Severe Weather, Chinese Academy of Meteorological Sciences, Beijing, China, [6]NOAA-CESSRST, City University of New York, New York, NY, USA, [7]Key Laboratory of Tropical Atmosphere-Ocean System (Sun Yat-sen University), Ministry of Education, Zhuhai, China, [8]Southern Marine Science and Engineering Guangdong Laboratory, Zhuhai, China

Abstract The physical and optical properties of aerosols and the change of planetary boundary layer height (PBLH) are of great scientific significance for the study of atmospheric environment and air quality. This paper intends to present integrated observations of aerosol physical-optical characteristics and PBLH properties under different air pollution levels in Shouxian (National Climatology Observatory (32°26' N, 116°47' E)), China. The combined measurements of ground-based Lidar and Cloud-Aerosol Lidar and Infrared Pathfinder Satellite Observation (CALIPSO) are analyzed from December 2016 to November 2017 in this study. Results show that the extinction coefficients decrease significantly with height below 2 km. The extinction coefficients below 1 km, the aerosol optical depth (AOD), and the PBLH increase with the aggravation of pollution. The daily average aerosol extinction coefficient near the surface is about 0.78 km^{-1}, the AOD is 0.87 ± 0.33 m (mean ± std, the same below), and the PBLH is 827 ± 132 m in polluted conditions ($PM_{2.5}$ > 115 μg m^{-3}). With the increase in pollution and the decrease in PBLH, more aerosols are accumulated at a lower height. The daily average ratios of AOD below PBLH (AOD_{PBLH}) to total AOD (AOD_{tot}) are about 64% in polluted conditions. According to the CALIPSO-observed aerosol vertical profile, aerosols are identified for about 20.54% of the vertical space below 6 km altitude under polluted conditions. The spherical fine particles with lower particulate depolarization ratio (PDR, 79% of the PDR is <0.2), lower color ratio (CR, 64% of the CR is <0.75), and stronger scattering ability are dominant in 0~2 km.

1. Introduction

Aerosols physical-optical properties of aerosols and the change of planetary boundary layer height (PBLH) are of great scientific significance for the study of atmospheric environment and air quality. Aerosols directly influence the amount and spectral distribution of the incoming solar radiation and the Earth's radiation-energy budget by scattering and/or absorbing the solar light (Ackerman & Toon, 1981; Charlson et al., 1992; Hansen et al., 1997; Luo et al., 2019). Indirectly, aerosols affect the radiation budget and climate through their impact on cloud microphysical processes as cloud condensation nuclei (Dubovik & King, 2000; Eck et al., 2012; Twomey, 1977; Twomey et al., 1984). Considering the spatial heterogeneity of aerosols at different heights, the analysis of vertical aerosol distributions can contribute to a better understanding of regional PBLH characteristics. Further, the vertical distribution characteristics of aerosols can affect the vertical profile of atmospheric radiation heat, thus changing the stability of the atmosphere, affecting the convective and turbulent motion (Bellouin et al., 2020; Chung et al., 2012; Johnson et al., 2008). Therefore, the detection of vertical aerosol distribution is of great significance.

The planetary boundary layer (PBL) is the lowest portion of the troposphere, which affects the exchanges of heat, momentum, and pollutants between the surface and the free troposphere (Garratt, 1994). The dispersion and dilution of pollutants are dynamically controlled by atmospheric motion (e.g., wind and turbulence) within the PBL (Stull, 1988). The PBL structures/processes not only regulate the horizontal dispersion and transport of aerosols,

but also influence the upward diffusion of aerosols and the exchange of cleaner air from above (Li et al., 2017; X. Yang et al., 2016). The shallow PBL has been found to be partially responsible for several pollution episodes in China (Quan et al., 2014; Su et al., 2018; Ye et al., 2016), and the shallower PBL also coincides with higher scattering extinction at low altitude (T. Z. Sun et al., 2019), Meanwhile, high aerosol loading may result in less heating to the atmosphere and radiative forcing to the surface (X. Yang et al., 2016), which in turn further depresses the PBL and exerts feedback on pollution (Y. Gao et al., 2015; Miao et al., 2016; X. Yang et al., 2016).

The ground-based Lidar has been proved to be one of the powerful tools to monitor optical properties of aerosols and clouds, as well as the PBL structures with high temporal and spatial resolution in the vertical direction (Baars et al., 2016). Therefore, Lidar has been widely used in the study of aerosol extinction vertical profiles and the investigation of urban air pollution (Chew et al., 2016; Q. Liu et al., 2017; Wong et al., 2017). In addition to ground-based Lidar detection, the spaceborne Lidar is also an effective means to obtain atmospheric aerosol information. The Cloud-Aerosol Lidar with Orthogonal Polarization (CALIOP) sensor carried on the polar-orbit Cloud-Aerosol Lidar and Infrared Pathfinder Satellite Observations (CALIPSO) satellite is the primary data source of large-scale and long-term vertical distribution characteristics of global aerosols and clouds (Winker et al., 2013; Yu et al., 2010). CALIPSO can effectively identify cloud components and determine aerosol layers and types.

In recent years, some researchers have analyzed the spatial distribution of aerosols by using ground-based Lidar and the CALIPSO satellite, and further verified the quality of CALIPSO aerosol data via the comparison with ground-based observations showing good consistency (Chiang et al., 2011; Solanki & Singh, 2014). Also, aerosol types were validated in some researches. Previous studies have validated different types of aerosols from CALIPSO Level-2 data sets by comparing them with the ground-based elastic Lidar, Raman Lidar, and aerosol robot network (AERONET), respectively (Burton et al., 2013; Mona et al., 2009; Pappalardo et al., 2010; Wu et al., 2014). These results showed the best consistency of dust types, but the moderate agreement of the polluted continental type of aerosols. Moreover, Wu et al. (Wu et al., 2014) have found that the cloud-aerosol discrimination (CAD) algorithm of CALIPSO works well except in the case of heavy aloft smoke plumes that are partially discriminated as clouds. The aerosol classification results observed from CALIPSO have been directly used by several studies to support the identification of aerosol air masses of specific types (W. Sun et al., 2013; Y. Yang et al., 2012).

The combination of ground-based and spaceborne Lidar has become the development trend of atmospheric aerosol detection (Gupta et al., 2021; Shen & Cao, 2020; Zhu et al., 2019). However, previous studies have rarely discussed the vertical profile changes of aerosol and PBLH under different pollution conditions when inhalable ground particles are the primary pollutants. Therefore, based on the ground-based Lidar and CALIPSO satellite, this paper explores the vertical distribution characteristics of aerosol particles under different pollution levels in China's Inland Cities (Shouxian National Climatology Observatory), which is of great scientific significance to reveal the spatial characteristics of aerosol and boundary layer state in inland cities of China. Herein, we present a study on the vertical distributions of aerosols under different pollution levels in Shouxian from December 2016 to November 2017. We try our best to demonstrate the following key points studied: (a) Make observation-based analysis of the PBLH variations and their relationship with $PM_{2.5}$ under different pollution conditions; (b) Characterize vertical distribution of aerosol types and physical-optical properties (extinction, depolarization ratio, and color ratio) under the different pollution days, by integrating the ground-based lidar, space-borne lidar (CALIPSO), satellite MODIS, ground $PM_{2.5}$ data set, etc. This paper is organized as follows. Section 2 presents the study areas, the data and the main methods used in this study. Section 3 shows the results and discussion. Finally, the conclusion and perspective are given in Section 4.

2. Instruments, Data, and Methodology

2.1. Ground-Based Lidar Instrument

The ground-based Lidar used in this observation experiment is a single wavelength Mie scattering Lidar (made by Anhui Institue Of Optics and Fine Mechanics, Chinese Academy of Sciences), which is located in Shouxian National Climatology Observatory, a county in Huainan, Anhui, China (Figure 1). The system transmits short pulses at 532 nm with a 20 Hz repetition rate, and the spatial resolution is 15 m. The Lidar profiles were obtained with a 5-min or 3-min interval. In the study of aerosol extinction profiles and PBLH characteristics, the one-year observation data from December 2016 to November 2017 are adopted, and the data with the cloud under

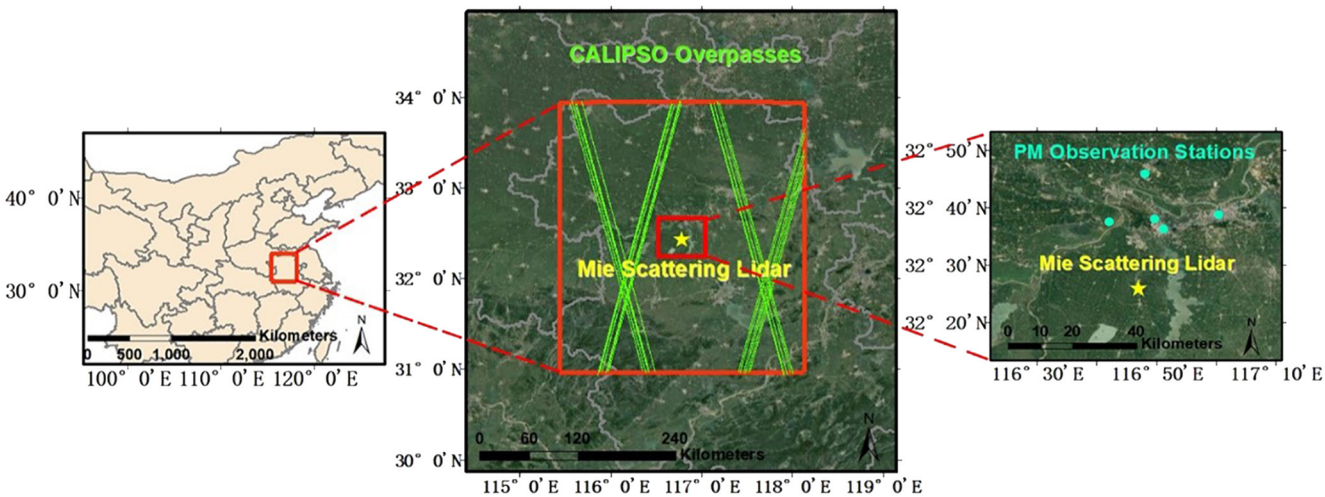

Figure 1. Map of the Shouxian, the location of Mie Scattering Lidar (32°26' N, 116°47' E), the CALIPSO overpasses (green lines) and the range of CALIPSO overpasses (red box).

3 km and rainy days are strictly removed. The height of low cloud is easily misjudged as PBLH, resulting in retrieval errors. Thus, it is necessary to remove the days with low clouds under 3 km. A total of 162-day profiles finally remained. The Lidar data corrections are essential to retrieve the aerosol extinction coefficient, including the range square correction, overlap correction, after-pulse correction, and background noise subtraction (Cao et al., 2013). After the Lidar data corrections, the aerosol extinction coefficient was obtained using the Fernald method (Fernald, 1984). In this inversion, the reference height is set at a height with negligible particle load (Balis et al., 2006), and the Lidar ratio (LR) is set at 50 (Fan et al., 2019; F. Y. Mao et al., 2012).

The aerosol optical depth (AOD) is calculated by integrating the extinction coefficient from the surface to the reference height excluding clouds, reflecting the attenuation of the sunlight-induced by aerosols. In this paper, if the extinction coefficient above 3 km is greater than that of the surface, it is considered that there are clouds above 3 km. The extinction coefficient is used to determine whether there are cloud changes with time and surface extinction coefficient. When we calculate the daily average AOD, we exclude the times in the day when there are clouds. The extinction coefficient data obtained from the Lidar were used to calculate the AOD remaining 149 days, which contain at least 5-hr data in one day after excluding clouds.

Aerosols are generally more abundant within the boundary layer than the upper atmosphere, thus for Lidar systems, the backscattered Lidar signals within the PBL are much higher than those in the free troposphere. Based on this fact, several methods have been employed to determine the PBLH from Lidar data. Many studies showed that the retrieved PBLH of Lidar is in good consistency with the radiosonde (Hennemuth & Lammert, 2006; Sawyer & Li, 2013). In this study, we choose the gradient method (GRA) (Comeron et al., 2013; Flamant et al., 1997; Hennemuth & Lammert, 2006; Hoff et al., 1996; W. Wang et al., 2016), standard deviation method (STD) (Hooper & Eloranta, 1986; Menut et al., 1999), and wavelet covariance transform method (WCT) (Cohn & Angevine, 2000; Deng et al., 2014; Granados-Munoz et al., 2012) to estimate the PBLH where the Lidar range corrected signal (RCS) abruptly decreases. The detailed inversion methods can be consulted from the paper discussed by Qu et al., who considered that all these three ways can reveal the characteristics of PBLH (Qu et al., 2017). In this study, the minimum PBLH is set at 500 m where the Lidar starts to collect full backscatter signals due to the limitation of the geometric overlap function. The maximum PBLH is set at 2,700 m to save computing time and avoid cloud contamination. Due to the low signal-to-noise ratio (SNR) of Mie scattering Lidar, this automatic inversion method may produce wrong values in some cases. We have checked the whole data and removed the data that are considered to be inaccurate. Finally, the daily data have been processed with Gaussian smoothing method, and the smooth window width is 10.

Table 1
Statistics of Pollution Days Used Different Data During the Study Period

Pollution level	Excellent	Moderate	Slightly polluted	Polluted
$PM_{2.5}$ concentration (μg m^{-3})	0∼35	35∼75	75∼115	>115
Lidar (days)	25	86	39	12
CALIPSO (days)	15	37	18	10

2.2. Satellite Products

CALIOP is a satellite-borne Lidar instrument carried on the CALIPSO, which can observe vertical aerosol profiles. The CALIOP Level-2 version 4.20 aerosol profile products and Vertical Feature Mask (VFM) products are downloaded from NASA's website (https://eosweb.larc.nasa.gov/project/CALIPSO) during the study period. These two data have a horizontal resolution of 5 km and a vertical resolution of 60 and 30 m below 8.2 km, respectively (Omar et al., 2009). Both data products are selected between 115.44–118.14°E and 30.96–33.94°N over the study region (Figure 1). A total number of 80 CALIPSO overpasses are available for the analysis, and the overpasses are further separated according to the pollution levels in Shouxian. In this study, some parameters closely associated with aerosol optical and microphysical properties are employed from profile products: extinction coefficients at 532 nm, total backscatter coefficient (TBC) at 532 nm, backscatter coefficient at 1,064 nm, and particulate depolarization ratio (PDR) profile at 532 nm.

Backscattering coefficient (0∼0.05 km^{-1} sr^{-1}) and PDR (0∼1) values are filtered with valid range limits of their magnitude, provided with the data product (Lakshmi et al., 2020). Because the extinction coefficient, backscattering coefficient and other parameters in the level-2 aerosol profile data are obtained from the Level-1 data through the correlation algorithm, there are many kinds of errors in the conversion process, eventually leading to the inaccuracy of level-2 data parameters. Therefore, it is necessary to carry out quality control to reduce errors using CALIPSO data (Campbell et al., 2013; Gautam et al., 2009; Redemann et al., 2012). The data quality control procedures are applied as follows: (1) $-100 \leq$ CAD score ≤ -50; CAD routine separates clouds and aerosols. The CALIOP reports CAD scores in the range of −100 to 0 for aerosols and 0 to +100 for clouds using the CALIOP cloud aerosol discrimination algorithm. The larger absolute value of the CAD score indicates higher confidence in the featured classification. The Range of CAD scores setting in this paper not only ensures the validity of the data to a certain extent but also avoids the lack of research data caused by the strict screening conditions. (2) The value of bits 1st-3rd of atmospheric volume description is 3. The data type of Atmospheric volume description (AVD) is a 16-bit integer, which reflects the detection type (cloud or aerosol or no signal), its subtype, the corresponding confidence level, etc. The 1st-3rd bits of AVD are feature types, and the value is 3 representing aerosol data. (3) The Extinction quality control (QC) 532 = 0 or Extinction QC = 1. The value of Extinction QC is related to the preset and change of Lidar ratio in the inversion process of extinction coefficient. Generally, when the value is 0 or 1, the inversion result is the most reliable. (4) Extinction Coefficient Uncertainty ≤10. When the uncertainty is ≥90, it indicates that the obtained data are not accurate. The VFM product uses a cloud-aerosol classification and recognition algorithm and aerosol layer classification algorithm to identify the received signals, and each bin range is characterized by a single 16-bit integer. Therefore, we decode these integer data to obtain different flags. In version 4.20, aerosols are divided into six subtypes: clean marine (CM), desert dust (DD), polluted continental/smoke (PC/SE), clean continental (CC, also referred to as clean background), polluted dust (PD, dust mixed with anthropogenic aerosols such as biomass burning smoke or urban pollution), elevated smoke (SE, smoke which is elevated above the PBL [2.5 km]), and dusty marine (DM, dust mixed with marine aerosol) (Boiyo et al., 2018; Kim et al., 2018).

2.3. Auxiliary Data

The observed $PM_{2.5}$ concentration data are sourced from the China Environmental Monitoring Center (CEMC). There are five monitoring stations in Huainan, with an average distance of 26 km away from the Lidar. The CEMC provides the hourly average data and the average of these five monitoring stations. According to the new air quality standard of $PM_{2.5}$ detection network of China (http://www.pm25china.net/), the six pollution conditions are classified by the 24-hr average $PM_{2.5}$ concentrations, including excellent condition (0∼35 μg m^{-3}), good condition (35∼75 μg m^{-3}), slightly polluted (75∼115 μg m^{-3}), moderately polluted (115∼150 μg m^{-3}), heavily polluted (150∼250 μg m^{-3}), and seriously polluted (>250 μg m^{-3}). Since few data are available in the moderately polluted, heavily polluted, and seriously polluted conditions, we consider these three conditions into one category, which is called the polluted condition. The number of days for each pollution level is shown in Table 1.

The AOD product from MODIS satellite sensor (MCD19A2-v6) is used in the present study to retrieve the daily AOD. MCD19A2 is a Multi-angle Implementation of Atmospheric Correction (MAIAC) Land AOD Level-2

gridded product having a high spatial resolution of 1 km, which integrates MODIS Terra and Aqua images. It offers daily basis AOD for land at two different wavelength bands, that is, 470 nm (blue band) and 550 nm (green band). AOD was selected at 550 nm (green band) for the same study period, and the grid data are averaged with a 5-km range away from the Lidar location. MCD19A2 is available for free download from the MODIS website (https://modis-land.gsfc.nasa.gov/MAIAC.html). Total 93-day MODIS data are further matched with Lidar data.

3. Results and Discussion

In this section, we analyze main statistical results of aerosols and PBLH under different pollution levels. The characteristics of aerosols extinction and AOD under the different pollution conditions are provided in Section 3.1. The relationship of $PM_{2.5}$ and AOD is also discussed. Section 3.2 presents the statistics of PBLH and the percentages of AOD below PBLH to total AOD. Besides, the TBC, PDR, and CR characteristics are given in Section 3.3. Furthermore, Section 3.4 presents the proportions of different aerosol types and their variation with altitude. In Sections 3.1–3.4, the statistical characteristics of different parameters of aerosol are analyzed. In Section 3.5, we further show the characteristics of these parameters in a case and discuss the impact of background meteorological parameters.

3.1. Aerosols Extinction Profiles and AOD Changes Under Different Pollution Conditions

Aerosol optical characteristics are critical physical parameters that reflect the aerosol concentration and chemical composition and are widely used in aerosol mode verification and improvement (M. Gao et al., 2018; Oikawa et al., 2018). The aerosol extinction coefficient is one of the essential aerosol optical parameters, reflecting the characteristics of the aerosol extinction. The extinction coefficient profiles at 532 nm observed from ground-based Lidar and space-borne CALIOP are averaged and smoothed accordingly under the excellent, good, slightly polluted, and polluted conditions, respectively. CALIPSO data use sea-level height, while Lidar data use the actual ground height of Shouxian county. The average elevation of Shouxian is only 21 m, so the height matching was ignored in the data processing. However, due to the overlapping height of the ground-based Lidar system, which is around 500 m, the derived optical properties of aerosols may not be correct near the surface. Meanwhile, as the CALIOP instrument is an active Lidar sensor, decaying signals can influence the quality of aerosol profiles, especially in the near-surface (L. Y. Wang et al., 2020).

The aerosol extinction coefficient profiles are shown in Figure 2. The extinction coefficients of the CALIPSO satellite are slightly different from that of Lidar, but the overall trends are the same. Obviously, the extinction coefficients decrease significantly with height below 2 km and increase with the aggravation of pollution near the surface. Besides, the differences of extinction coefficients mainly exist below 1 km among those different conditions. In Figure 2a, the extinction coefficients are ~0.78, 0.57, 0.39, and 0.21 km^{-1} on the ground, in polluted, slightly polluted, good, and excellent conditions, respectively. The extinction coefficients decrease fleetly below 1 km in polluted conditions, while it changes slightly in excellent conditions. Generally, the average extinction coefficients observed by Lidar are smaller than those observed by CALIPSO. For results from CALIPSO, the extinction coefficients in excellent and good conditions are a little larger than that in slightly polluted and polluted conditions above 1 km (Figure 2b). This phenomenon is not obvious as observed by Lidar. The main reason for the difference between the two data sets is that the observation time and site are different.

AOD is seen as an important indicator for evaluating aerosol concentration and atmospheric pollution reflecting the extinction characteristics of aerosols in the whole atmosphere column. As shown in Figure 3, the daily average Lidar AOD during the study period is 0.65 ± 0.33 (mean ± std, the same below), ranging from 0.18 to 1.70. The more serious the pollution, the greater the AOD. The mean value of Lidar AOD is up to 0.87 ± 0.33 on polluted days. What's more, the average values of AOD are 0.75 ± 0.33, 0.66 ± 0.33, and 0.36 ± 0.11 in slightly polluted, good, and excellent conditions, respectively.

In order to check the accuracy of Lidar AOD, we run a linear regression with MODISAOD data. The result shows that the slope of the regression equation is 1.20 (Figure 3b). The Pearson correlation coefficient is 0.83, and they are considered to be highly correlated. P-values are substantial at the 1% confidence level for all the linear fits, thus we consider that the values of Lidar AOD are accurate. The correlation between Lidar AOD with $PM_{2.5}$ concentration was tested (Figure 3c). The bibliography agrees that AOD is positively related to $PM_{2.5}$ (Shao et al., 2017; Q. Yang et al., 2019). Our results also agree with it, and the correlation coefficient (0.45) is

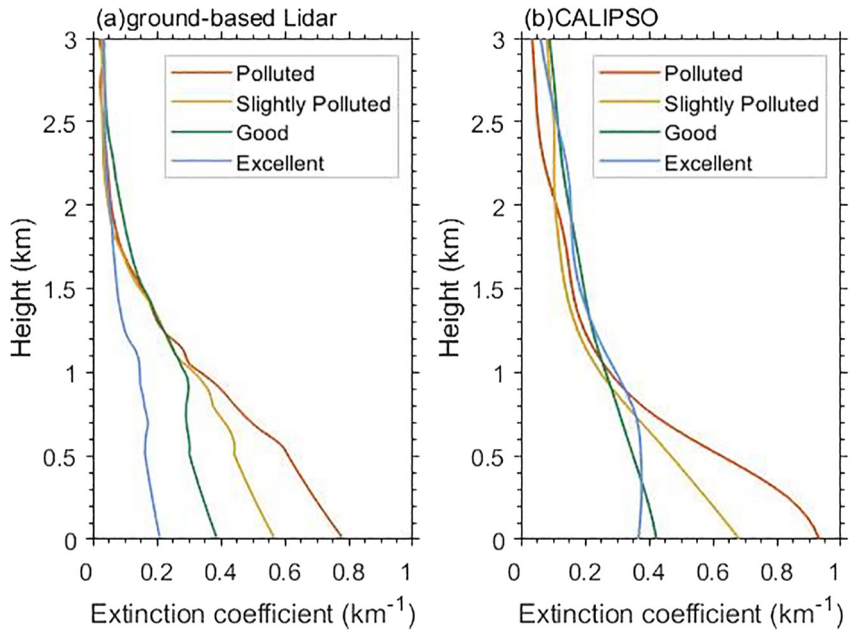

Figure 2. Extinction coefficient profiles for ground-based Lidar and CALIPSO under different pollution levels.

higher than that in the previous study in Hefei (0.33∼0.38) (Q. Yang et al., 2019). However, many factors can influence their relationship. For example, $PM_{2.5}$ reflects particle concentration near the ground surface, while AOD represents the entire atmospheric column. In addition, $PM_{2.5}$ mainly represents the dry mass concentration of fine particles, which is hardly affected by water and coarse particles, but the AOD value might also include the influence of water vapor and coarse particles. The detailed analysis is shown in Figure 4.

We analyze the correlation between the Lidar-derived AOD and CALIPSO-measured color ratio (CR). CR is defined as the ratio of the intensity of backscatters at 1,064 nm and that of total backscatters at 532 nm; the larger color ratio usually indicates larger particle sizes or coarse-mode particles. As shown in Figure 3d, AOD is negatively correlated with CR, and the correlation coefficient (R) is −0.46. The higher AOD corresponds to smaller color ratios, which indicate the fine-mode particles. In fact, when the particle size is close to the wavelength of incident light, the contribution of this particle to extinction is greater than that of other size particles (Seinfeld & Pandis, 2012). Previous field observations showed that PM_1 makes the main contribution to extinction, which can reach more than 70% (Bergin et al., 2001). Thus, the fine particles with small CR and the high extinction make a greater contribution to AOD.

The correlations among $PM_{2.5\sim10}/PM_{10}$ ratio, relative humidity (RH) and $PM_{2.5}$/AOD ratio are shown in Figure 4 through the scatter plots. A previous study proved that the $PM_{2.5}$/AOD ratio is a good parameter to measure the relationship between $PM_{2.5}$ concentration and AOD (Zheng et al., 2017). The ratio of $PM_{2.5\sim10}/PM_{10}$ represents the proportion of coarse particles. We find that $PM_{2.5}\sim_{10}/PM_{10}$ ratio and RH both are negatively correlated with $PM_{2.5}$/AOD ratio. When the proportion of monitored coarse particles increases, the contribution of coarse particles to AOD increases. Accordingly, the contribution of fine particles to AOD reduces, and decreases the $PM_{2.5}$/AOD ratio. Moreover, when the humidity is high, the aerosol would be humidified and the particles tend to contain more water. In fact, the water contained in the particles will contribute a lot to AOD and make the value of AOD larger (Covert et al., 1972). The active sensor of the ground-based Lidar can monitor elevated aerosols from range-resolved aerosol distribution and compensate the disadvantage of the satellite retrievals of column AOD only. However, the concentration of $PM_{2.5}$ is dry mass concentration, where the water contained in the particles is evaporated and contributes little to $PM_{2.5}$ mass concentration in the measurements (Q. Yang et al., 2019). That is to say, high humidity makes the particles in the air contain more water, which makes the AOD higher, but the impact on the concentration of $PM_{2.5}$ is relatively weak, resulting in a relatively lower $PM_{2.5}$/AOD ratio.

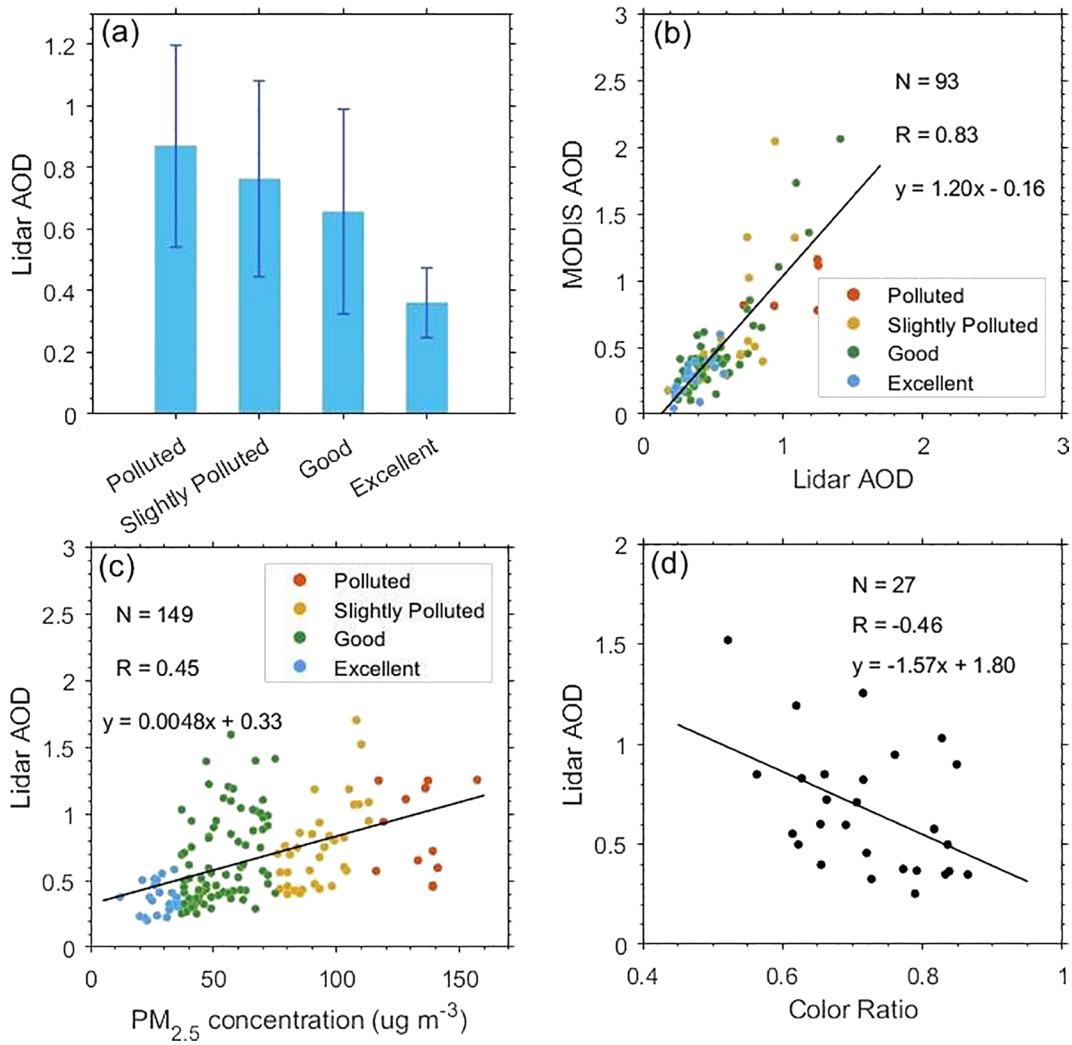

Figure 3. (a) The daily average aerosol optical depth (AOD) observed by ground-based Lidar under different pollution levels; (b) the correlation between the AOD of ground-based Lidar and the AOD of MODIS; (c) the correlation between the $PM_{2.5}$ concentration and the AOD of ground-based Lidar; and (d) the correlation between the color ratio and the AOD of ground-based Lidar.

3.2. PBLH Characteristics Over Shouxian in Different Air Quality

The variations in aerosol concentrations can affect the stability of the PBL, and the vertical aerosol distribution plays a vital role in PBL development (Su et al., 2020). Meanwhile, air pollutants released from non-buoyant ground sources, including aerosols, dust, and other gaseous pollutants, are restricted within the boundary layer (Petaja et al., 2016). Therefore, the dispersion and transport of lower tropospheric particles mainly depend on the PBLH (Tyagi et al., 2017; Zilitinkevich et al., 2012). Consequently, the determination of PBLH is of great significance to the evaluation of air pollution events. In this study, we apply the GRA, STD, and WCT methods to calculate the PBLH. The following paragraphs will identify and discuss the statistical characteristics of PBLH over Shouxian.

The box plot in Figure 5a shows and compares statistical characteristics of PBLH under the excellent, good, slightly polluted, and polluted conditions, which is calculated by the GRA, STD, and WCT methods, respectively. The results show that the annual variation of daily PBLH is between 593 and 1,765 m, and the annual average of PBLH is 1,042 ± 254 m, which is in excellent agreement with other experimental data in China (Deng et al., 2016; Du et al., 2013). The PBLHs in polluted conditions are the lowest with the average value of 827 m and are the most stable with a standard deviation of 132 m. This was consistent with previous field observations

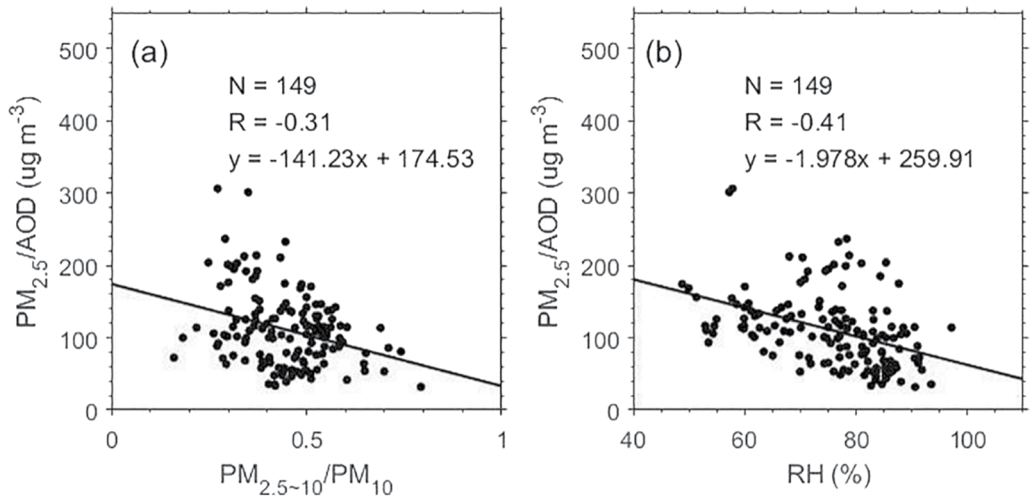

Figure 4. (a) The correlation between the $PM_{2.5}$/AOD ratio and the $PM_{2.5\sim10}/PM_{10}$ ratio; and (b) the correlation between the $PM_{2.5}$/AOD ratio and the relative humidity (RH).

that the boundary layer would be very low during heavy $PM_{2.5}$ pollution conditions with high extinction (Luan et al., 2018; Uno et al., 2014). Moreover, the PBLH values in good and excellent conditions are similar with the average value of 1,085 ± 253 m and 1,161 ± 275 m, respectively. Generally, the value of PBLH shows more significant variability under the states with higher PBLH, while the value of PBLH is less variable when the PBLH is low. Obviously, reduction of PBLH occurs with increased air pollution, and this result is coherent with the other studies (Lou et al., 2019; Miao et al., 2019). It can be explained by the two-way feedback effect between aerosol pollution and PBL structure (Zhang et al., 2020). The particles reduce the incident solar radiation and reduce the surface heating, resulting in a decrease of turbulent mixing and the reduction of PBLH. In turn, PBLH is associated with the highest height that the surface particles can reach, thus the shallow PBL limits particles to a low height and further facilitate the particulate matter accumulation.

The seasonal variation of PBLH under different pollution conditions are analyzed in Figure 5b. The results indicate that the PBLH decreases with the aggravation of pollution in each season. The seasonal average PBLH is

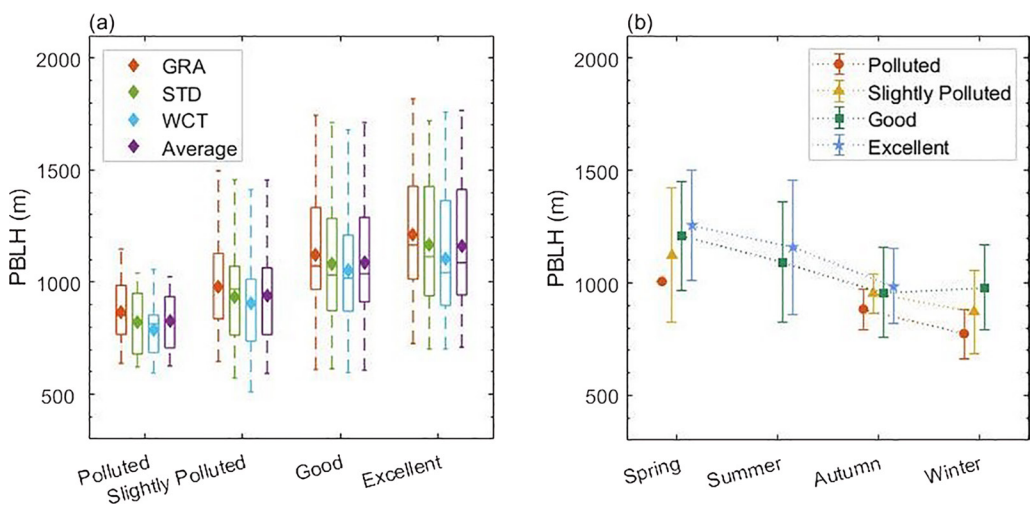

Figure 5. (a) The planetary boundary layer height (PBLH) calculated by the GRA, STD, and WCT methods under excellent, good, slightly polluted and polluted particulate pollution conditions, respectively. The bottom and top of the box are the first and third quartiles, and the band inside the box is the median and the diamond is the average. The whisker is the lowest (highest) datum within 1.5 interquartile ranges (IQR) of the lower (upper) quartile; (b) Seasonal variation of PBLH (three-method average) under different pollution conditions.

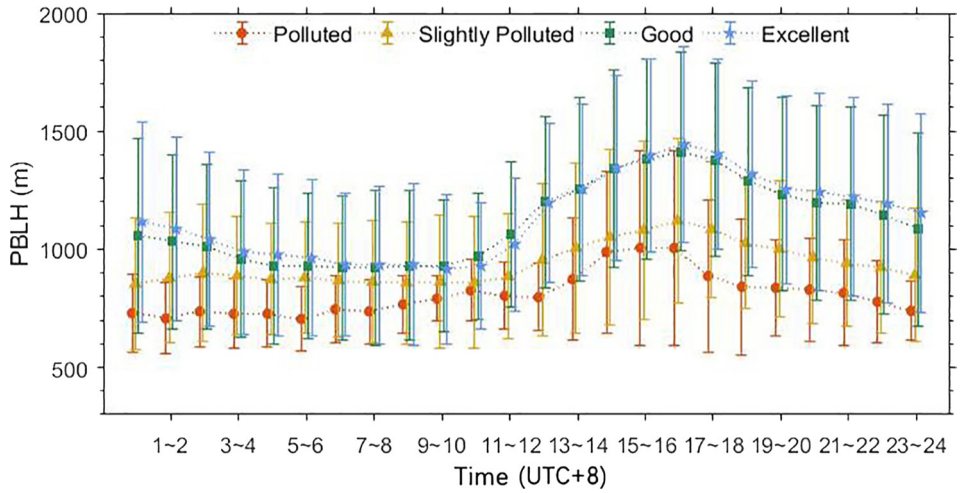

Figure 6. Daily variation of planetary boundary layer height (three-method average and hourly average) under different pollution conditions.

lowest in winter, but higher in spring and summer. Jiang et al. (Jiang et al., 2014) also found that the maximum PBL has the highest value of l.77 km in spring over Nanjing city in China. Although the increase in surface temperature is beneficial to increase the PBLH, the increase in relative humidity will reduce it (Jiang et al., 2014). The lower average value of the PBLH in summer may be due to the fact that the region is in the plum rainy season (W. S. Mao et al., 2008), with high relative humidity. Thus, too humid air will aggravate the air quality, resulting in the inability of the PBL to rise to a higher height.

The daily variation of PBLH (three-method average) and the related standard deviation in different pollution conditions is depicted in Figure 6. The PBLH changes with sunrise and sunset and reaches its maximum in the afternoon (16:00~17:00) in all the conditions. Lv et al. (Lv et al., 2020) also observed the PBLH peak at around 14:00 based on WRF-Chem during January and July in 2017 in North China Plain. Moreover, the diurnal cycles show similar patterns in good and excellent conditions and generally minimum in the mornings (08:00~09:00), respectively. However, the PBLH is at the lowest level at night in slightly polluted and polluted conditions. From 00:00 to 12:00, the PBLH remains relatively stable in slightly polluted conditions, and it slightly fluctuates in polluted conditions. Relative to excellent conditions, PBLH peak in polluted conditions see a big fall by 439 m, followed in slightly polluted conditions with a decrease of 324 m.

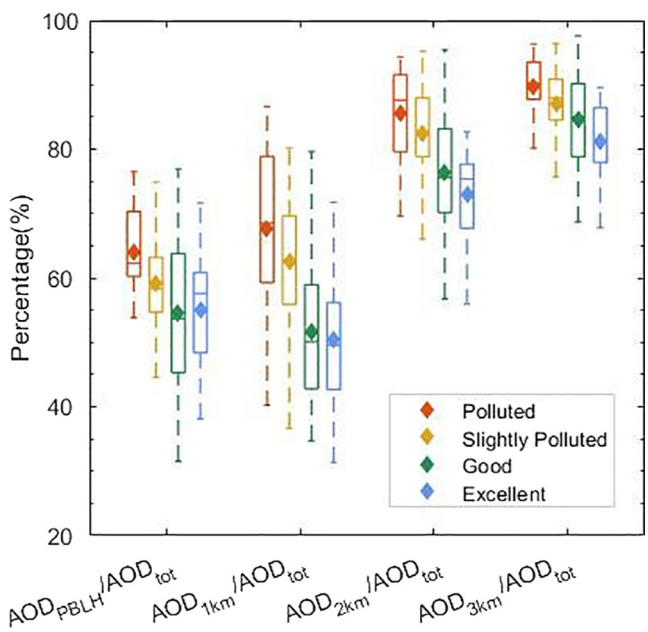

Figure 7. The percentages of aerosol optical depth (AOD) below average PBLH (AOD_{PBLH}), AOD below 1 km (AOD_{1km}), AOD below 2 km (AOD_{2km}), and AOD below 3 km (AOD_{3km}) to total AOD (AOD_{tot}) calculated by ground-based Lidar under different pollution levels.

Figure 7 shows the ratios of AOD below PBLH, 1 km, 2 km, and 3 km to total AOD calculated by ground-based Lidar, respectively. During the study period, the annual ratio of AOD below PBLH to total AOD is about 57%, indicating that more than half of the aerosols are concentrated below PBLH. He et al. (He et al., 2008) found that ~64% of the monthly mean AOD was contributed by aerosols within the PBL from May 2003 to June 2004 in Hong Kong. The daily average ratios of AOD below PBLH to total AOD are about 64%, 59%, 55%, and 55% in polluted, slightly polluted, good, and excellent conditions, respectively. Moreover, the annual percentages of AOD below 1 km, 2 km, and 3 km to total AOD are about 55%, 78%, and 85%, respectively. This is consistent with other views that most aerosols exist below 3 km. Overall, the percentages of AOD below 1 km, 2 km, and 3 km to total AOD increase with the aggravation of pollution, prove that aerosols mainly exist under lower height on more polluted days

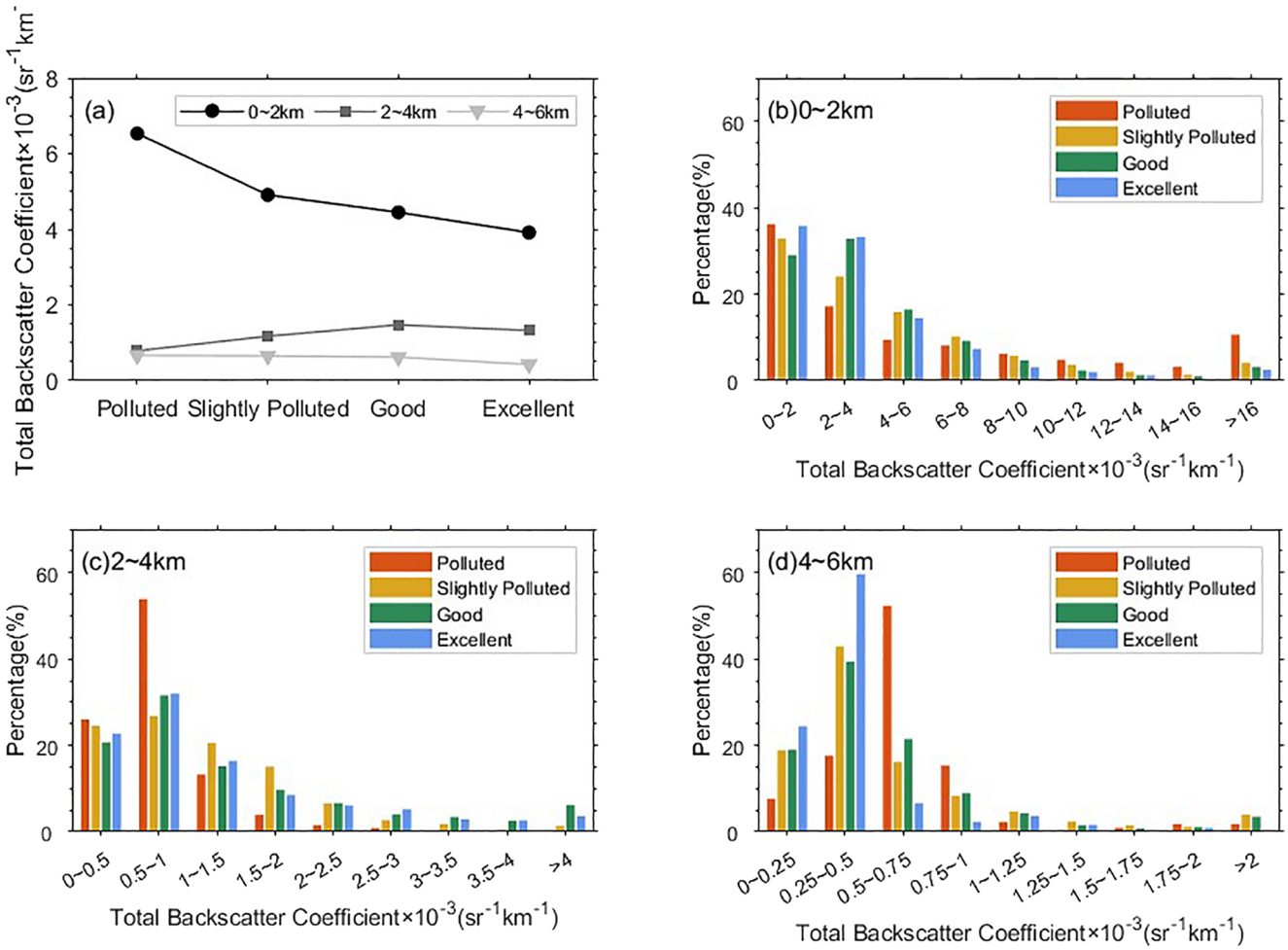

Figure 8. (a) The average total backscatter coefficient at different layers in different pollution conditions; and the frequency distributions of total backscatter coefficient in different pollution conditions at (b) 0∼2 km, (c) 2∼4 km, and (d) 4∼6 km.

3.3. TBC, PDR, and CR Characteristics in Different Pollution Levels

Based on the CALIPSO data, the temporal and spatial variations of aerosols in Shouxian are analyzed from three aspects: backscatter coefficient, particulate depolarization ratio, and color ratio. The height is divided into three height layers, including low layer (0∼2 km), middle layer (2∼4 km), and high layer (4∼6 km). The average value of each height layer is then calculated to further analyze the vertical distribution characteristics of the above three parameters during different pollution periods. The backscatter coefficient is an essential parameter in CALIPSO Level-2 aerosol profile products. According to the research conducted by Liu et al. (Q. Liu et al., 2017), the aerosol-related TBC at 532 nm varies from 8.0×10^{-4} to 4.5×10^{-3} km^{-1} sr^{-1}, except when there are optically thick aerosol layers or optically thin clouds (particularly cirrus). As shown in Figure 8a, the annual mean values of TBC generally diminish with increases in height, which are 5.2×10^{-3} km^{-1} sr^{-1}, 1.2×10^{-3} km^{-1} sr^{-1}, and 6×10^{-4} km^{-1} sr^{-1} from low layer to high layer, respectively. The mean value in the low layer is significantly higher than that in the other two layers, indicating that the scattering ability of particles is very strong at 0∼2 km, especially on polluted days with its average value up to 7.1×10^{-3} km^{-1} sr^{-1}. The TBC increases with the deterioration of air quality in the low and high layer, while there is a modest slowdown in the middle layer. This result denotes that more aerosols exist in low layer with low PBLH when the air is seriously polluted, causing less aerosols in the middle layer. On average, about 90% of TBCs are $<10.6 \times 10^{-3}$ km^{-1} sr^{-1} at 0∼2 km (Figure 8b), while TBCs are more concentrated in a small range at 2∼4 km and 4∼6 km (Figures 8c and 8d), with 90% of TBCs concentrated in 0∼2.8×10^{-3} km^{-1} sr^{-1} and 0∼1.1×10^{-3} km^{-1} sr^{-1}, respectively.

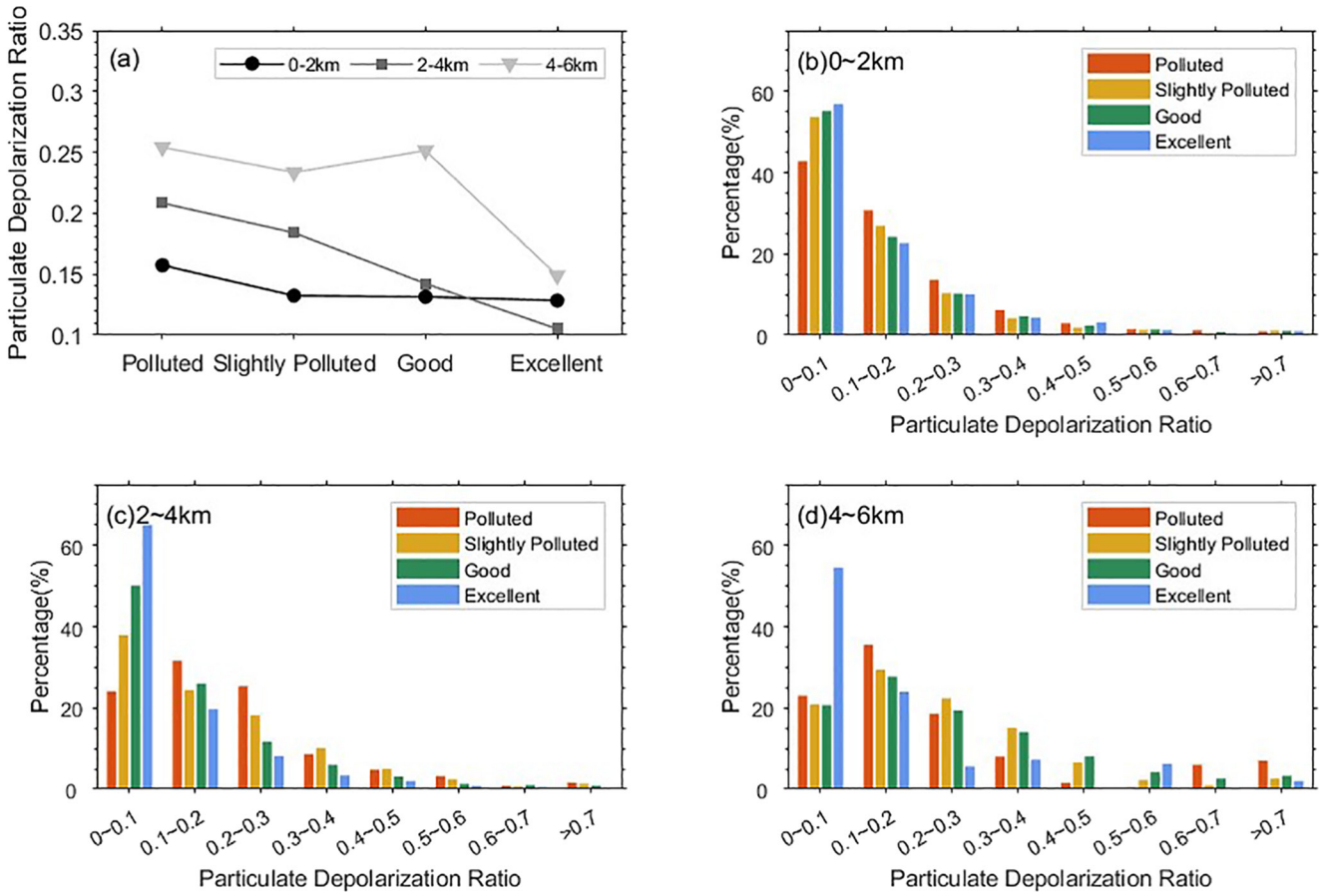

Figure 9. (a) The average particulate depolarization ratio at different layers in different pollution conditions; and the frequency distributions of particulate depolarization ratio in different pollution conditions at (b) 0∼2 km, (c) 2∼4 km, and (d) 4∼6 km.

The PDR is used to distinguish spherical or nonspherical particles (Bi, Lin, Liu, & Zhang, 2018; Bi, Lin, Wang, et al., 2018; Winker et al., 2007). Higher PDR values suggest greater amounts of nonspherical particles (such as dust), and smoke resulting in small PDR values. Omar et al. considered PDR >0.2 as a dust criterion from other aerosol types (Omar et al., 2009). Figure 9a depicts that the mean value of the PDR increases with the height, except in excellent conditions, indicating that the amount of nonspherical particles increases with the height. For excellent conditions, most PDR are less than 0.1, which do not vary apparently with height increases (Figure 9a). For 0∼2 km, the frequency distributions of PDR are similar in different pollution levels (Figure 8b), because the aerosols under PBLH are mainly originated from local and surrounding areas. However, at 2∼4 km and 4∼6 km, the difference of average values (Figure 9a) and frequency distribution (Figures 9c and 9d) is obvious among different pollution levels. The aerosols in higher altitude mainly comes from different areas through long-distance transportation. Approximately 79% and 72% of the PDR values are smaller than 0.2, respectively, at 0∼2 km and 2∼4 km, indicating the dominance of spherical aerosols at the low layer and middle layer (Figures 9b and 9c). Whereas at 4∼6 km, about 52% of the PDR values are smaller than 0.2, which represents that both spherical and irregular particles present at higher altitude (Figure 9d).

The CR represents the size of particles. According to Liu et al. (Z. Liu et al., 2008), the peak values of frequency distribution of CR is ∼0.2, ∼0.35, and ∼0.8 for marine aerosols, smoke aerosols, and dust, respectively. The larger values are due to the larger sizes of dust particles. As shown in Figure 10a, the CR changes regularly, decreasing with the reduction of the height and the worsening of pollution. It may be because that most aerosols are dust with large CR at a higher altitude, which can be seen in Figure 10. Aerosol particles appear with smaller sizes when the $PM_{2.5}$ concentration is higher. However, in the polluted period, the values are roughly the same at middle and high layers. What's more, approximately 64% of the CR is <0.75 at 0∼2 km, and the proportion decreases with the increases in height, which is 51% at 2∼4 km and 43% at 4∼6 km.

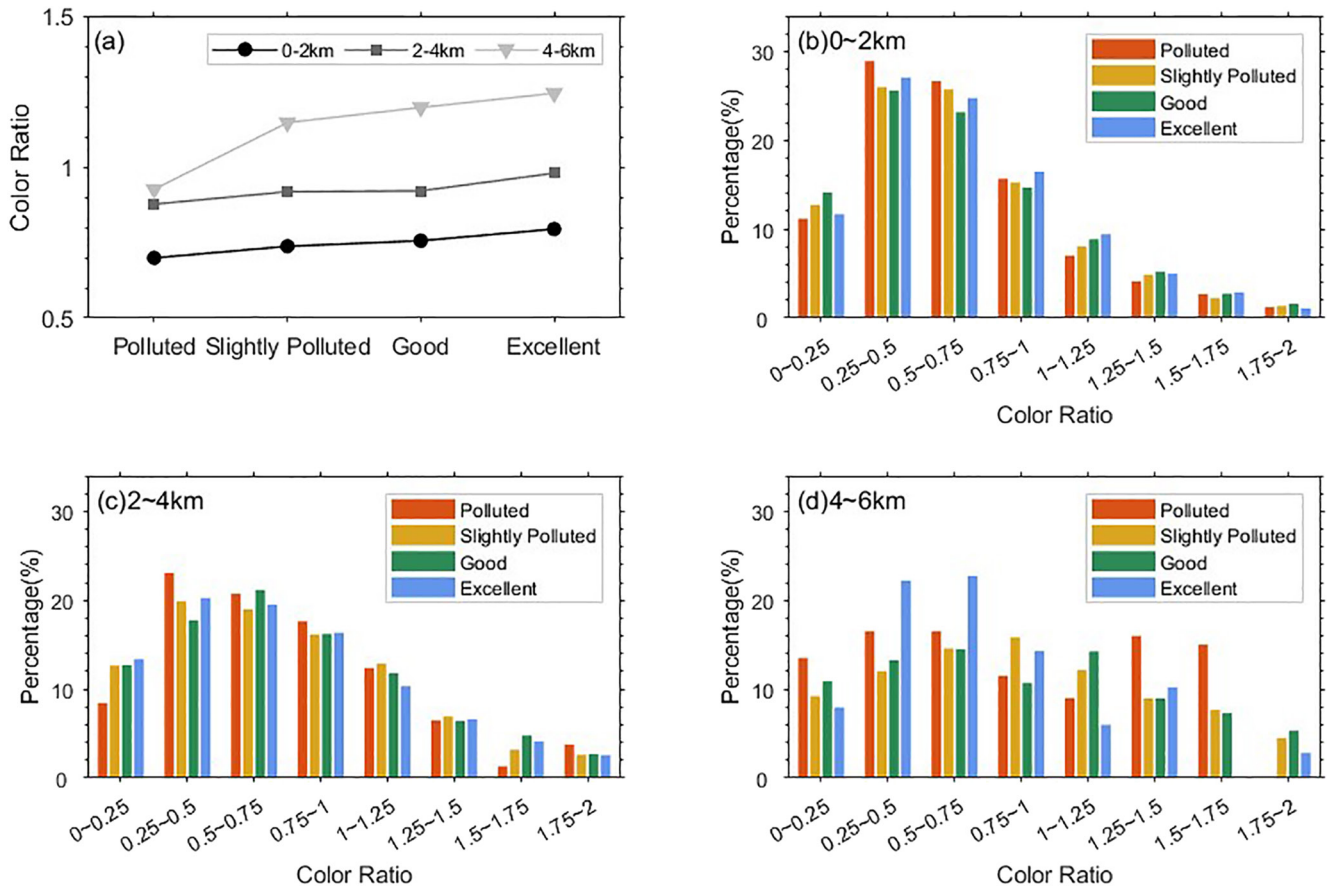

Figure 10. (a) The average color ratio at different layers in different pollution conditions; and the frequency distributions of color ratio in different pollution conditions at (b) 0∼2 km, (c) 2∼4 km, and (d) 4∼6 km.

3.4. Proportion of Aerosols of Different Types Under Various Pollution Conditions

In order to obtain the frequency distribution of different aerosol types observed over the Shouxian, we decoded the aerosol classification flag of 10∼12 bit obtained from the VFM files (day + night) over the study domain (Figure 1) during different pollution periods. The occurrence frequency of aerosol in the whole sky (including five types of aerosols, clear air, cold and no signal) of CALIPSO overpasses under 6 km is calculated and presented in Table 1. We can note that the pollution conditions are not greatly consistent with the space proportion of aerosol in the atmosphere (Table 2). The proportion of all aerosols in polluted conditions is a little lower than that of slightly polluted and good conditions. That is because the $PM_{2.5}$ concentration is monitored on the ground surface. Besides, at the higher altitude, the aerosol loading in slightly polluted and good conditions are larger than that in polluted conditions shown in Figure 11. During the study year, the main aerosol types identified are PD, PC/SE, DD, and SE, which accounted for ∼9.47%, ∼4.57%, ∼3.31%, and ∼2.75%, respectively.

Table 2
The Proportion of Occurrence of Different Aerosol Types in the Whole Cross Section of CALIPSO Tracks Under 6 km

Period	All aerosol percentage	Aerosol type				
		PD	DD	PC/SE	SE	CC
Polluted	20.54%	11.16%	3.25%	4.95%	0.98%	0.20%
Slightly Polluted	21.99%	10.34%	3.94%	5.40%	1.65%	0.66%
Good	21.32%	9.99%	4.15%	3.59%	3.35%	0.24%
Excellent	16.47%	6.08%	0.54%	5.72%	3.76%	0.37%
Annual	20.46%	9.47%	3.31%	4.57%	2.75%	0.35%

PD are the predominant aerosol subtype and its percent contribution varied significantly with the pollution levels noticed in polluted condition (11.16%) followed by slightly polluted condition (10.34%), good (9.99%), and excellent (6.08%). PD, as also reported in earlier findings, was the major contributor to total AOD over South East China (Mehta et al., 2018). The PD concentration increases with the rise in pollution levels, and it is the opposite of SE concentration. Further, it is noticed that the DD concentration during the polluted period is smaller, occupying ∼3.25% than the slightly polluted period (3.94%) and good period (4.15%). This phenomenon is due to the fact that most polluted days are in winter and the DD concentration during the

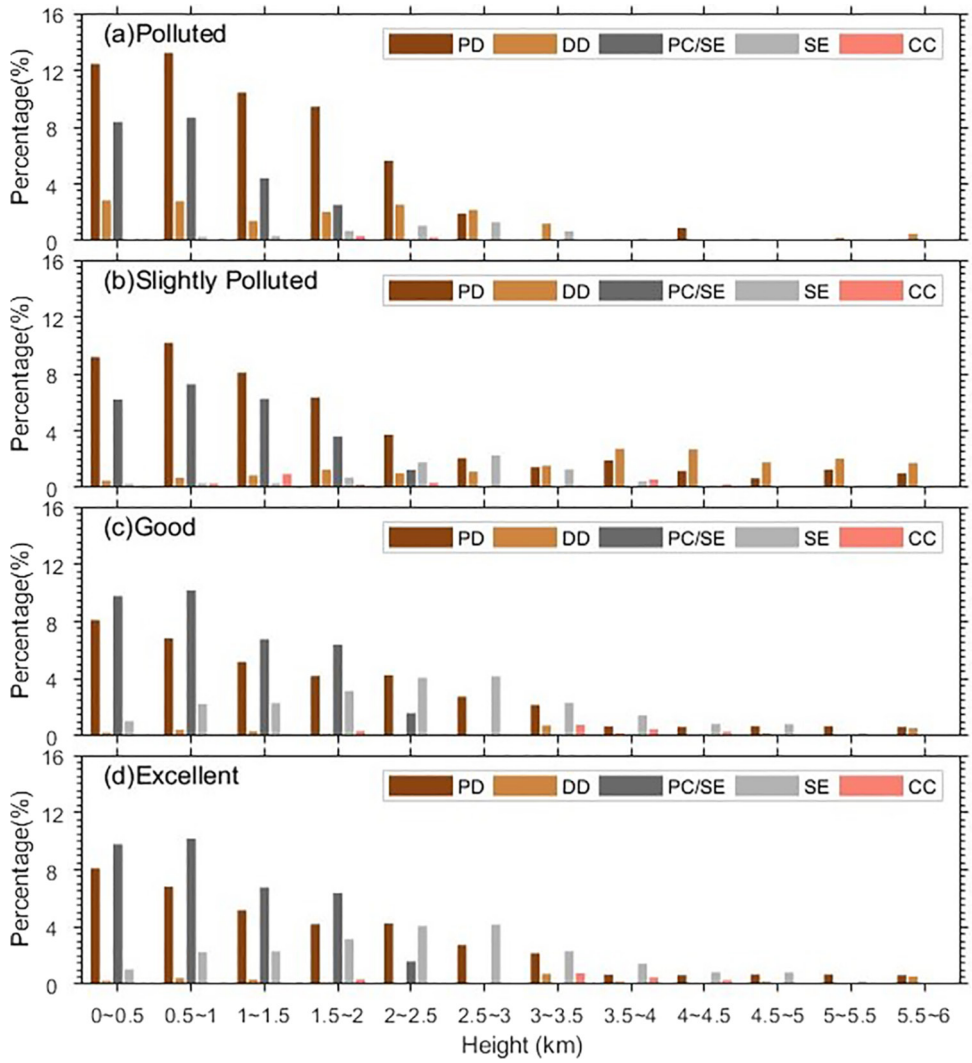

Figure 11. Frequency distribution of different aerosol subtypes during different periods and different heights under 6 km.

winter season is smaller (Mehta et al., 2018; Proestakis et al., 2018; Tan et al., 2014). In addition, the CM and DM type of aerosols have no contribution to the total aerosol distribution due to the geographical location away from the ocean environment.

Figure 11 displays the vertical distribution of these different aerosol types (expressed in percentage). About 96% of aerosols occur below 3 km during polluted days, which is obviously higher than that in the slightly polluted and good conditions. This further indicates that the low PBLH contributed significantly to heavy pollution events, leading to an increase in aerosol concentration near the ground. We can notice the maximum concentration of PD and PC/SE aerosol types are most observed at an altitude of 0.5~1 km. At the same time, the concentrations of the two types gradually decrease with an increase in height. The PC/SE only appears below 2.5 km due to the discrimination mechanism of the VFM product that the aerosol is considered as SE type if the top of the aerosol layer is higher than 2.5 km. The SE type shows a unimodal distribution during each period with its peak highest not close to the surface but at an altitude of 2.5~3 km attributed to injection height of SE into the atmosphere (Mehta et al., 2018). There are few DD particles in excellent condition. However, the DD mainly appears at high altitudes during the slightly polluted period, and it is evenly distributed below 6 km during the good period.

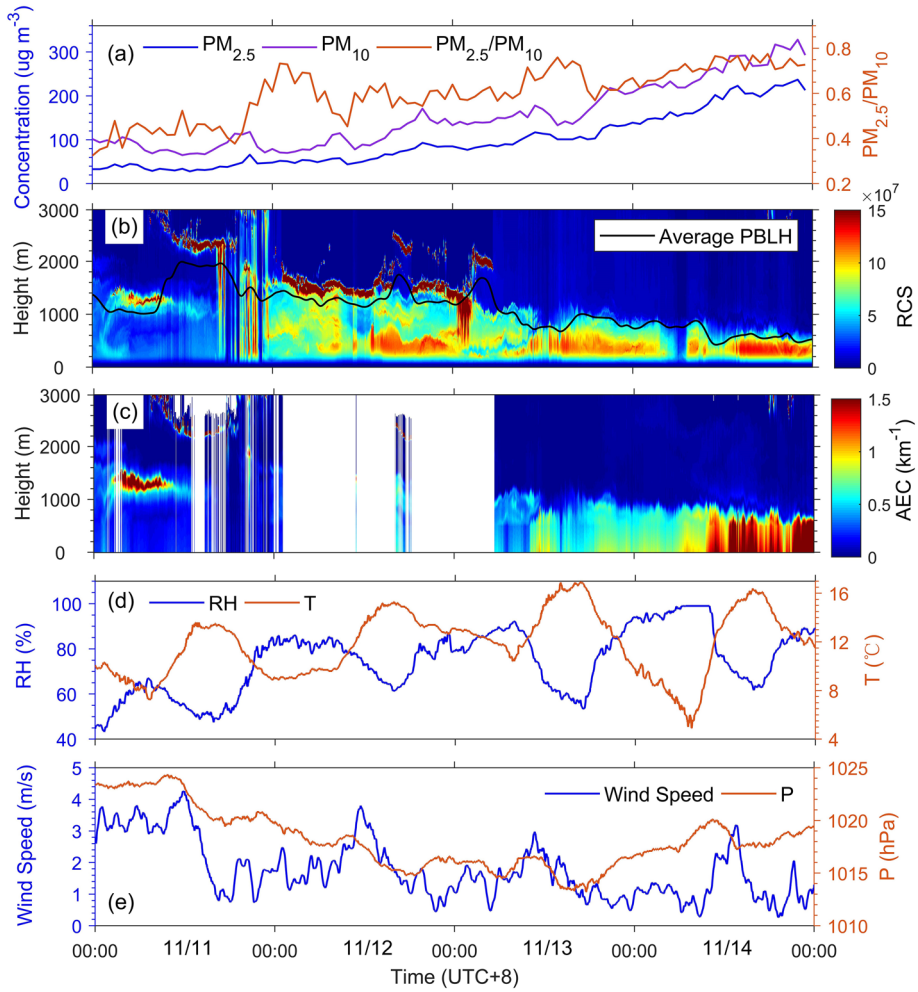

Figure 12. Time series from 00:00 UTC+8 on 11 November 2016 to 00:00 UTC+8 on 15 November 2016 of: (a) $PM_{2.5}$ and PM_{10} concentration, (b) range corrected signal and average planetary boundary layer height, (c) aerosol extinction coefficient, (d) surface relative humidity (RH) and temperature (T), (e) surface wind speed, (U) and pressure (P).

3.5. Case Study

In order to comprehensively analyze the mechanism of relationship among the $PM_{2.5}$ concentration, extinction coefficient, PBLH, and meteorological elements, we select a development episode from excellent conditions to heavy particle pollution within four consecutive days. As shown in Figure 12 a, the variation of $PM_{2.5}$ is consistent with that of PM_{10}. Along with this $PM_{2.5}$ concentration increase from average 38 μg m^{-3} on November 11 to average 185 μg m^{-3} on November14, it can be seen that PBLH drops markedly from 1,469 m to 644 m, simultaneously (Figure 12b). During this period, the aerosol extinction coefficient below PBLH rises by nearly 6-fold from 0.18 km^{-1} to 1.14 km^{-1} (Figure 12c), which is similar to the rate of $PM_{2.5}$. On one hand, as the emission increases, the total atmospheric pollutants increase, and the $PM_{2.5}$ concentration on the ground increases correspondingly. On the other hand, due to higher total atmosphere pollutants, increased extinction effect of sunlight reduces PBLH, thereby aerosols can only diffuse in the smaller volumes than before, making the near-surface $PM_{2.5}$ concentrations rise further. With the role of impact of aerosol on PBL, the near-surface concentration of $PM_{2.5}$ grows higher than that of initial PBL.

Besides PBLH, other factors, such as relative humidity, wind, weather patterns, and atmospheric stability, can affect aerosol concentrations. Generally, the temperature shows a rising trend (Figure 12d). The increase in temperature can contribute to the formation rate of aerosol chemical reaction and the formation of more secondary aerosols (Tsang et al., 1988). In addition, with the high relative humidity, aerosols are more likely to accumulate

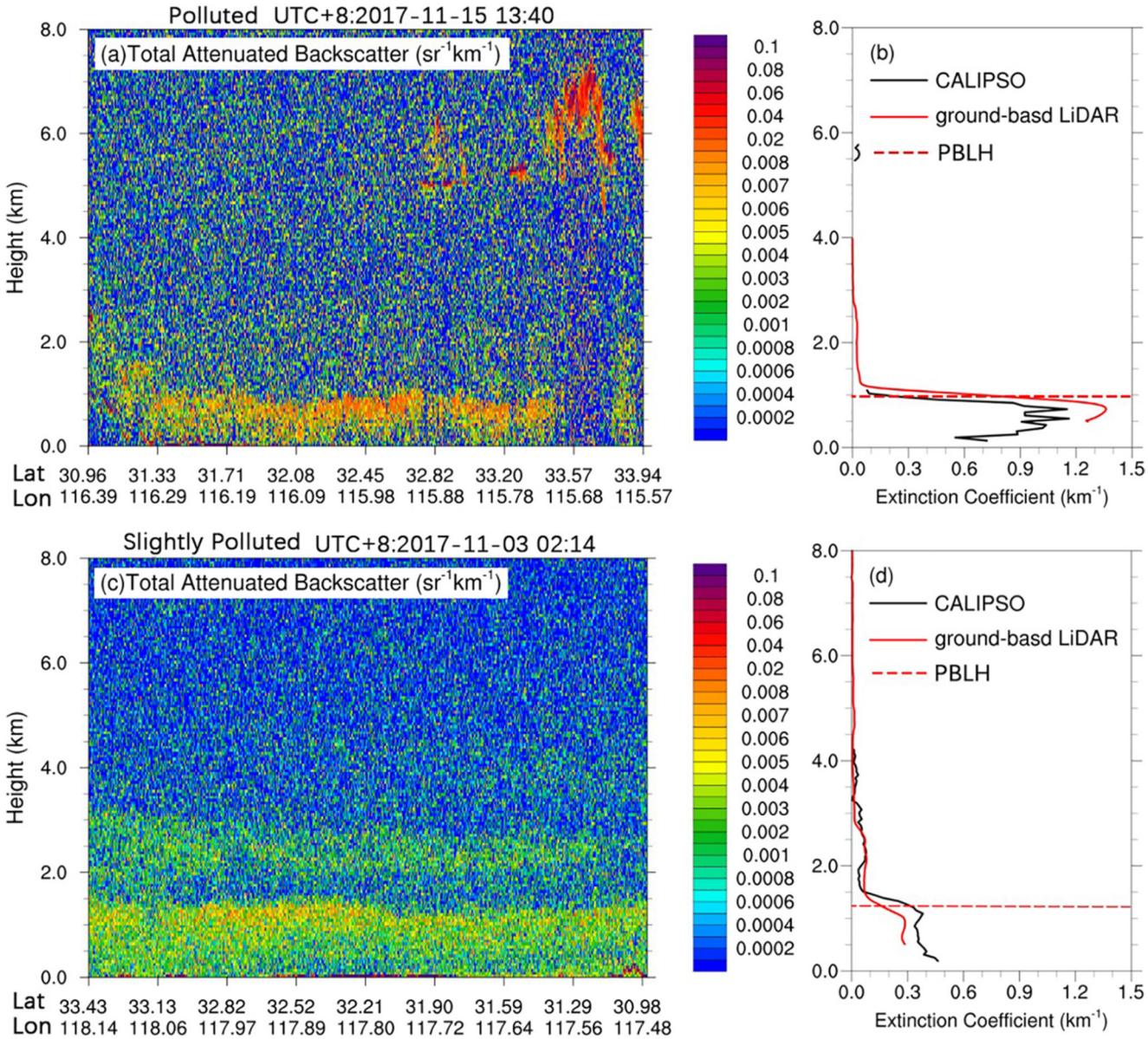

Figure 13. (a), (c) The vertical distribution of total attenuated backscatter coefficient and (b), (d) the average profile of the aerosol extinction coefficient and the planetary boundary layer height on 15 November 2017 and 03 November 2017, respectively.

through hygroscopic growth and accelerate liquid-phase and heterogeneous reactions to worsen aerosol pollution (Ervens et al., 2011; Kuang et al., 2016). Empirical relations of aerosol optical properties with relative humidity are widely presented in previous studies (Malm & Day, 2001; J. Sun et al., 2016). Therefore, as the relative humidity increases (Figure 12d), the scattering ability of the aerosol is enhanced. Accompanied by the reduction of PBLH, the wind speed and surface pressure generally decrease (Figure 12e). The shallow boundary layer, weak wind, and low pressure impose restrictions on the diffusion of pollutants as well as water vapor. Thus, less air diffusion and more particle formation lead to high aerosol concentration and high extinction coefficient below PBLH.

In order to further understand the vertical distribution of aerosols under different pollution conditions, November 15 (polluted day) and November 03 (slightly polluted day) are selected in this study. Figures 13a and 13c show the vertical profile of the total attenuated backscatter at 532 nm from the CALIPSO L1 product, which can show the distribution of aerosols directly. In Figure 13a, there are obvious green, orange, and red signals within 1 km

near the surface, and most of the backscattering intensity is 0.002–0.01 sr^{-1} km^{-1}, indicating heavy aerosol loadings. The blue color in the figure shows the gas molecules, and the backscattering coefficient is 0.0001∼0.0008 sr^{-1} km^{-1}. However, in 2∼8 km, there are still some green and a little orange color scattered distribution, and the backscattering coefficient is 0∼0.01 km sr^{-1} km^{-1}, indicating that aerosol and gas molecules are mixed in this height layer. Moreover, the CALIPSO detected a cloud at 5∼7.5 km, shown as red color, and below it is blue due to the weak satellite detection signal. In Figure 13c, most aerosols exist below 3 km with green color, and there are two aerosol layers separately at 0∼1.5 km and 2∼3 km. Above the aerosol layer, the backscatter is weaker on the slightly polluted day than that on the polluted day. The maximum of the backscattering coefficient does not appear at the surface but near the top of the aerosol layer or the top of the bottom aerosol layer when two layers exist. The average extinction coefficients of ground-based Lidar within 2 hr of CALIPSO crossing and the CALIPSO L2 products are shown as the red and black solid line, respectively (Figures 13b and 13d). Basically, the two profiles of extinction coefficient show similar tendency.

Further, the PDR characteristic, CR characteristic, and types of aerosols are compared in Figure 14. The PDR and CR on November 15 are a little smaller than that at the bottom aerosol layer and much smaller than that at the upper aerosol layer on November 03. It implies that most spherical and fine particles are present in the atmosphere, but more irregular and coarser particles exist on the slightly polluted day. PD and PC/SE are the predominant aerosol subtype on November 15 and at the bottom aerosol layer on November 03. However, there is a tremendous amount of PD with some DD at the upper aerosol layer on November 03. The results are consistent with the statistics shown in Figure 11.

4. Conclusions

In this study, we analyze the vertical distribution characteristics in Shouxian during December 2016 ∼ November 2017, including optical characteristics of aerosols and aerosol types. The PBLH characteristics in different pollution conditions are discussed. At last, their correlations with meteorological elements are analyzed through a case study. The conclusions are as follows.

Generally, the extinction coefficients decrease significantly with height below 2 km and increase with the aggravation of pollution near the surface. Meanwhile, the mean value of TBC on 0∼2 km (5.2×10^{-3} km^{-1} sr^{-1}) is significantly higher than that on 2∼4 km (1.2×10^{-3} km^{-1} sr^{-1}) and 4∼6 km (6×10^{-4} km^{-1} sr^{-1}). The aerosol extinction coefficient near the surface observed by ground-based Lidar is up to 0.78 km^{-1} and the AOD is 0.87 ± 0.33 in polluted condition.

The PBLH is relatively lower when the ground $PM_{2.5}$ concentration is higher. The annual ratio of AOD below PBLH to total AOD is about 57%, and it is up to 64% in the polluted condition. The percentages of AOD below 1 km, 2 km, and 3 km to total AOD increase with the aggravation of pollution, which imply that aerosols mainly exist under lower height on more polluted days owing to lower PBLH.

Spherical fine particles with lower PDR (79% of the PDR is <0.2) and lower CR (64% of the CR is <0.75) are dominant in 0∼2 km. Both the scattering ability of particles and the percentage of irregular fine particles are larger in polluted conditions than in slightly polluted and pristine conditions.

In addition, the results reveal that aerosols exist in about 20.54% of the vertical space under 6 km in polluted condition observed by CALIPSO in the vertical section. Aerosols mainly exist under low PBLH in polluted conditions, resulting in a lower ratio in polluted conditions when compared with in slightly polluted (21.99%) and good (21.32%) conditions. The polluted dust is the dominant aerosol subtype observed through the study period (9.47%), and its concentration increases with the rise in pollution levels.

The results presented in this study mainly describe the aerosol physical-optical properties in the vertical direction and provide the relationship with PBLH. However, the study time is just one year, and future work will explore the characteristics and rules during longer years.

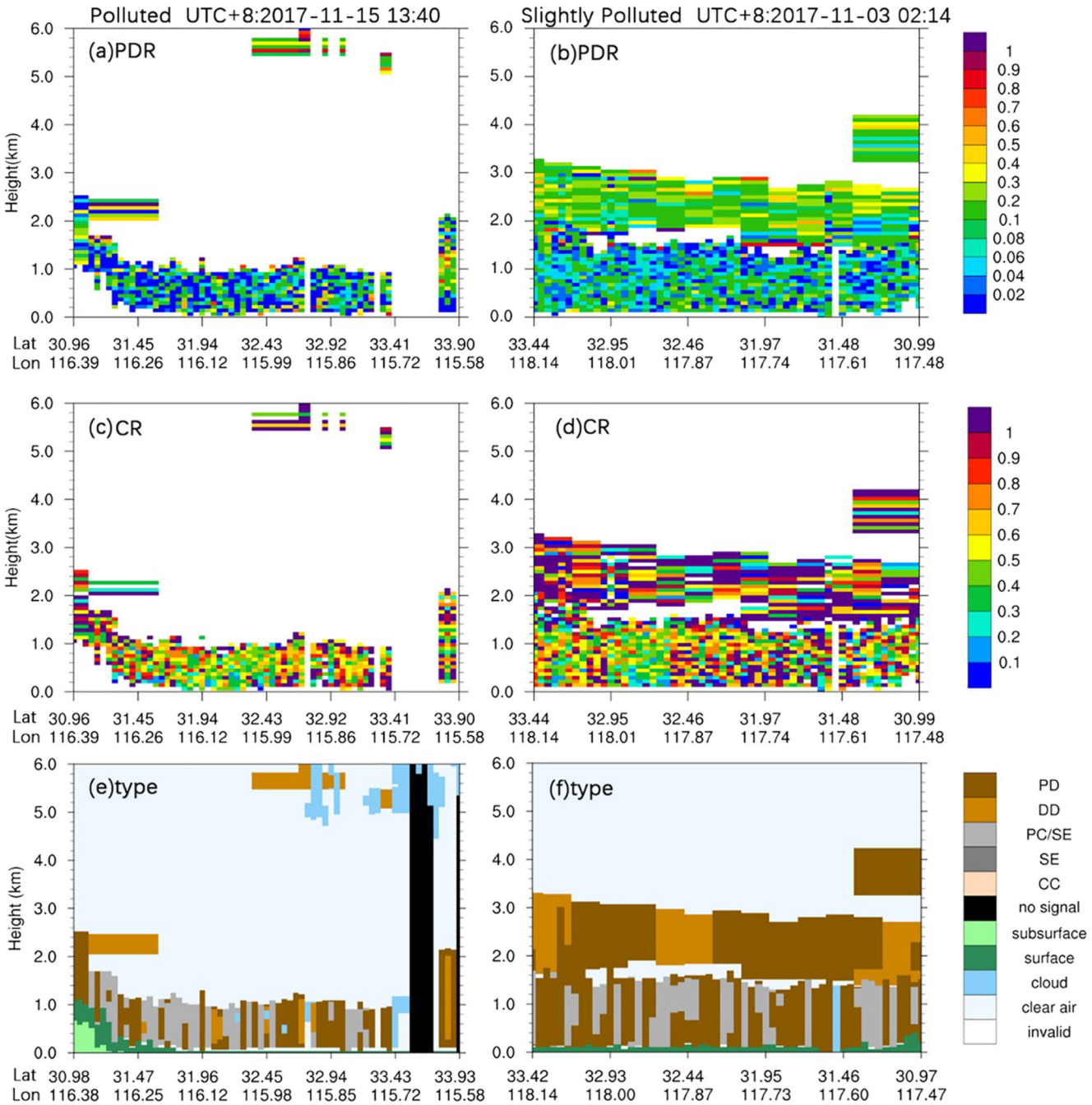

Figure 14. (a and b) PDR, (c and d) CR and (e and f) the aerosol types on 15 November 2017 and 03 November 2017, respectively.

Data Availability Statement

The CALIPSO data were obtained from NASA Langley Research Center Atmospheric Science Data Center through the websites https://eosweb.larc.nasa.gov/project/CALIPSO. The MODIS data were provided by Land Processes Distributed Active Archive Center, from https://lpdaac.usgs.gov/products/mcd19a2v006/. The meteorological data (RH, T, Wind, and P) can be found from China National Meteorological Science Data Center (http://data.cma.cn/data/cdcdetail/dataCode/A.0012.0001_340.html). The ground-based Lidar data, PM data, and results data of all Figures in this paper have been uploaded to the Baidu Netdisk (under https://pan.baidu.com/s/1klBurI3P7S6JL-bEOINAQw, password: hg1o).

Acknowledgments
This work was jointly supported by the National Science Foundation of China (Grant Nos. 41775026, 42027804, 41075012 and 40805006). We also thank the anonymous reviewers for their constructive comments that have helped us to improve the manuscript. We are very grateful to the three anonymous reviewers for their insights, which are of vital importance to improve the quality of the article.

References

Ackerman, T. P., & Toon, O. B. (1981). Absorption of visible radiation in atmosphere containing mixtures of absorbing and nonabsorbing particles. *Applied Optics*, *21*(20), 3661–3667. https://doi.org/10.1364/ao.20.003661

Baars, H., Kanitz, T., Engelmann, R., Althausen, D., Heese, B., Komppula, M., et al. (2016). An overview of the first decade of Polly(NET): An emerging network of automated Raman-polarization lidars for continuous aerosol profiling. *Atmospheric Chemistry and Physics*, *16*(8), 5111–5137. https://doi.org/10.5194/acp-16-5111-2016

Balis, D., Amiridis, V., Kazadzis, S., Papayannis, A., Tsaknakis, G., Tzortzakis, S., et al. (2006). Optical characteristics of desert dust over the East Mediterranean during summer: A case study. *Annales Geophysicae*, *24*(3), 807–821. https://doi.org/10.5194/angeo-24-807-2006

Bellouin, N., Quaas, J., Gryspeerdt, E., Kinne, S., Stier, P., Watson-Parris, D., et al. (2020). Bounding global aerosol radiative forcing of climate change. *Reviews of Geophysics*, *58*(1), 45. https://doi.org/10.1029/2019rg000660

Bergin, M. H., Cass, G. R., Xu, J., Fang, C., Zeng, L. M., Yu, T., et al. (2001). Aerosol radiative, physical, and chemical properties in Beijing during June 1999. *Journal of Geophysical Research*, *106*(D16), 17969–17980. https://doi.org/10.1029/2001jd900073

Bi, L., Lin, W. S., Liu, D., & Zhang, K. J. (2018). Assessing the depolarization capabilities of nonspherical particles in a super-ellipsoidal shape space. *Optics Express*, *26*(2), 1726–1742. https://doi.org/10.1364/oe.26.001726

Bi, L., Lin, W. S., Wang, Z., Tang, X. Y., Zhang, X. Y., & Yi, B. Q. (2018). Optical modeling of sea salt aerosols: The effects of nonsphericity and inhomogeneity. *Journal of Geophysical Research: Atmospheres*, *123*(1), 543–558. https://doi.org/10.1002/2017jd027869

Boiyo, R., Kumar, K. R., & Zhao, T. L. (2018). Spatial variations and trends in AOD climatology over East Africa during 2002-2016: A comparative study using three satellite data sets. *International Journal of Climatology*, *38*, E1221–E1240. https://doi.org/10.1002/joc.5446

Burton, S. P., Ferrare, R. A., Vaughan, M. A., Omar, A. H., Rogers, R. R., Hostetler, C. A., & Hair, J. W. (2013). Aerosol classification from airborne HSRL and comparisons with the CALIPSO vertical feature mask. *Atmospheric Measurement Techniques*, *6*(5), 1397–1412. https://doi.org/10.5194/amt-6-1397-2013

Campbell, J. R., Reid, J. S., Westphal, D. L., Zhang, J. L., Tackett, J. L., Chew, B. N., et al. (2013). Characterizing the vertical profile of aerosol particle extinction and linear depolarization over Southeast Asia and the Maritime Continent: The 2007-2009 view from CALIOP. *Atmospheric Research*, *122*, 520–543. https://doi.org/10.1016/j.atmosres.2012.05.007

Cao, X., Wang, Z., Tian, P., Wang, J., Zhang, L., & Quan, X. (2013). Statistics of aerosol extinction coefficient profiles and optical depth using lidar measurement over Lanzhou, China since 2005–2008. *Journal of Quantitative Spectroscopy and Radiative Transfer*, *122*, 150–154. https://doi.org/10.1016/j.jqsrt.2012.09.016

Charlson, R. J., Schwartz, S. E., Hales, J. M., Cess, R. D., Coakley, J. A., Hansen, J. E., & Hofmann, D. J. (1992). Climate forcing by anthropogenic aerosols. *Science*, *255*(5043), 423–430. https://doi.org/10.1126/science.255.5043.423

Chew, B. N., Campbell, J. R., Hyer, E. J., Salinas, S. V., Reid, J. S., Welton, E. J., et al. (2016). Relationship between aerosol optical depth and particulate matter over Singapore: Effects of aerosol vertical distributions. *Aerosol and Air Quality Research*, *16*(11), 2818–2830. https://doi.org/10.4209/aaqr.2015.07.0457

Chiang, C.-W., Das, S. K., Shih, Y.-F., Liao, H.-S., & Nee, J.-B. (2011). Comparison of CALIPSO and ground-based lidar profiles over Chung-Li, Taiwan. *Journal of Quantitative Spectroscopy & Radiative Transfer*, *112*(2), 197–203. https://doi.org/10.1016/j.jqsrt.2010.05.002

Chung, C. E., Ramanathan, V., & Decremer, D. (2012). Observationally constrained estimates of carbonaceous aerosol radiative forcing. *Proceedings of the National Academy of Sciences of the United States of America*, *109*(29), 11624–11629. https://doi.org/10.1073/pnas.1203707109

Cohn, S. A., & Angevine, W. M. (2000). Boundary layer height and entrainment zone thickness measured by lidars and wind-profiling radars. *Journal of Applied Meteorology*, *39*(8), 1233–1247. https://doi.org/10.1175/1520-0450(2000)039<1233:blhaez>2.0.co;2

Comeron, A., Sicard, M., & Rocadenbosch, F. (2013). Wavelet correlation transform method and gradient method to determine aerosol layering from lidar returns: Some comments. *Journal of Atmospheric and Oceanic Technology*, *30*(6), 1189–1193. https://doi.org/10.1175/jtech-d-12-00233.1

Covert, D. S., Charlson, R. J., & Ahlquist, N. C. (1972). A study of the relationship of chemical composition and humidity to light scattering by aerosols. *Journal of Applied Meteorology*, *11*(6), 968–976. https://doi.org/10.1175/1520-0450(1972)011<0968:asotro>2.0.co;2

Deng, T., Deng, X. J., Li, F., Wang, S. Q., & Wang, G. (2016). Study on aerosol optical properties and radiative effect in cloudy weather in the Guangzhou region. *The Science of the Total Environment*, *568*, 147–154. https://doi.org/10.1016/j.scitotenv.2016.05.156

Deng, T., Wu, D., Deng, X. J., Tan, H. B., Li, F., & Liao, B. T. (2014). A vertical sounding of severe haze process in Guangzhou area. *Science China-Earth Sciences*, *57*(11), 2650–2656. https://doi.org/10.1007/s11430-014-4928-y

Du, C. L., Liu, S. Y., Yu, X., Li, X. M., Chen, C., Peng, Y., et al. (2013). Urban boundary layer height characteristics and relationship with particulate matter mass concentrations in Xi'an, Central China. *Aerosol and Air Quality Research*, *13*(5), 1598–1607. https://doi.org/10.4209/aaqr.2012.10.0274

Dubovik, O., & King, M. D. (2000). A flexible inversion algorithm for retrieval of aerosol optical properties from Sun and sky radiance measurements. *Journal of Geophysical Research*, *105*(D16), 20673–20696. https://doi.org/10.1029/2000jd900282

Eck, T. F., Holben, B. N., Reid, J. S., Giles, D. M., Rivas, M. A., Singh, R. P., et al. (2012). Fog- and cloud-induced aerosol modification observed by the Aerosol Robotic Network (AERONET). *Journal of Geophysical Research*, *117*, D07206. https://doi.org/10.1029/2011jd016839

Ervens, B., Turpin, B. J., & Weber, R. J. (2011). Secondary organic aerosol formation in cloud droplets and aqueous particles (aqSOA): A review of laboratory, field and model studies. *Atmospheric Chemistry and Physics*, *11*(21), 11069–11102. https://doi.org/10.5194/acp-11-11069-2011

Fan, W. Z., Qin, K., Xu, J., Yuan, L. M., Li, D., Jin, Z., & Zhang, K. F. (2019). Aerosol vertical distribution and sources estimation at a site of the Yangtze River Delta region of China. *Atmospheric Research*, *217*, 128–136. https://doi.org/10.1016/j.atmosres.2018.11.002

Fernald, F. (1984). Analysis of atmospheric lidar observations: Some comments. *Applied Optics*, *23*(5), 652–653. https://doi.org/10.1364/ao.23.000652

Flamant, C., Pelon, J., Flamant, P. H., & Durand, P. (1997). Lidar determination of the entrainment zone thickness at the top of the unstable marine atmospheric boundary layer. *Boundary-Layer Meteorology*, *83*(2), 247–284. https://doi.org/10.1023/a:1000258318944

Gao, M., Ji, D. S., Liang, F. C., & Liu, Y. (2018). Attribution of aerosol direct radiative forcing in China and India to emitting sectors. *Atmospheric Environment*, *190*, 35–42. https://doi.org/10.1016/j.atmosenv.2018.07.011

Gao, Y., Zhang, M., Liu, Z., Wang, L., Wang, P., Xia, X., et al. (2015). Modeling the feedback between aerosol and meteorological variables in the atmospheric boundary layer during a severe fog-haze event over the North China Plain. *Atmospheric Chemistry and Physics*, *15*(8), 4279–4295. https://doi.org/10.5194/acp-15-4279-2015

Garratt, J. R. (1994). Review: The atmospheric boundary layer. *Earth-Science Reviews*, *37*(1), 89–134. https://doi.org/10.1016/0012-8252(94)90026-4

Gautam, R., Liu, Z., Singh, R. P., & Hsu, N. C. (2009). Two contrasting dust-dominant periods over India observed from MODIS and CALIPSO data. *Geophysical Research Letters*, *36*, L06813. https://doi.org/10.1029/2008gl036967

Granados-Munoz, M. J., Navas-Guzman, F., Bravo-Aranda, J. A., Guerrero-Rascado, J. L., Lyamani, H., Fernandez-Galvez, J., & Alados-Arboledas, L. (2012). Automatic determination of the planetary boundary layer height using lidar: One-year analysis over southeastern Spain. *Journal of Geophysical Research*, *117*, D18208. https://doi.org/10.1029/2012jd017524

Gupta, G., Ratnam, M. V., Madhavan, B. L., Prasad, P., & Narayanamurthy, C. S. (2021). Vertical and spatial distribution of elevated aerosol layers obtained using long-term ground-based and space-borne lidar observations. *Atmospheric Environment*, *246*. https://doi.org/10.1016/j.atmosenv.2020.118172

Hansen, J., Sato, M., & Ruedy, R. (1997). Radiative forcing and climate response. *Journal of Geophysical Research*, *102*(D6), 6831–6864. https://doi.org/10.1029/96jd03436

He, Q., Li, C., Mao, J., Lau, A. K.-H., & Chu, D. A. (2008). Analysis of aerosol vertical distribution and variability in Hong Kong. *Journal of Geophysical Research*, *113*(D14), D14211. https://doi.org/10.1029/2008jd009778

Hennemuth, B., & Lammert, A. (2006). Determination of the atmospheric boundary layer height from radiosonde and lidar backscatter. *Boundary-Layer Meteorology*, *120*(1), 181–200. https://doi.org/10.1007/s10546-005-9035-3

Hoff, R. M., Guise-Bagley, L., Staebler, R. M., Wiebe, H. A., Brook, J., Georgi, B., & Dusterdiek, T. (1996). Lidar, nephelometer, and in situ aerosol experiments in southern Ontario. *Journal of Geophysical Research*, *101*(D14), 19199–19209. https://doi.org/10.1029/95jd03228

Hooper, W. P., & Eloranta, E. W. (1986). Lidar measurements of wind in the planetary boundary layer: The method, accuracy and results from joint measurements with radiosonde and Kytoon. *Journal of Climate and Applied Meteorology*, *25*(7), 990–1001. https://doi.org/10.1175/1520-0450(1986)025<0990:lmowit>2.0.co;2

Jiang, J., Zheng, Y. F., Liu, J. J., & Fan, G. G. (2014). Observational research on planetary boundary layer by lidar over Nanjing city. *Environmental Science & Technology*, *37*, 22–27.

Johnson, B. T., Heese, B., McFarlane, S. A., Chazette, P., Jones, A., & Bellouin, N. (2008). Vertical distribution and radiative effects of mineral dust and biomass burning aerosol over West Africa during DABEX. *Journal of Geophysical Research*, *113*(D17), D00C12. https://doi.org/10.1029/2008jd009848

Kim, M. H., Omar, A. H., Tackett, J. L., Vaughan, M. A., Winker, D. M., Trepte, C. R., et al. (2018). The CALIPSO version 4 automated aerosol classification and lidar ratio selection algorithm. *Atmospheric Measurement Techniques*, *11*(11), 6107–6135. https://doi.org/10.5194/amt-11-6107-2018

Kuang, Y., Zhao, C. S., Tao, J. C., Bian, Y. X., & Ma, N. (2016). Impact of aerosol hygroscopic growth on the direct aerosol radiative effect in summer on North China Plain. *Atmospheric Environment*, *147*, 224–233. https://doi.org/10.1016/j.atmosenv.2016.10.013

Lakshmi, N. B., Nair, V. S., & Babu, S. S. (2020). Assessment of the vertical distribution of speciated aerosol absorption over South Asia using spaceborne LIDAR and ground-based observations. *Remote Sensing of Environment*, *253*, 112164. https://doi.org/10.1016/j.rse.2020.112164

Li, Z. Q., Guo, J. P., Ding, A. J., Liao, H., Liu, J. J., Sun, Y. L., et al. (2017). Aerosol and boundary-layer interactions and impact on air quality. *National Science Review*, *4*(6), 810–833. https://doi.org/10.1093/nsr/nwx117

Liu, Q., He, Q. S., Fang, S. H., Guang, Y., Ma, C. Y., Chen, Y. H., et al. (2017). Vertical distribution of ambient aerosol extinctive properties during haze and haze-free periods based on the micro-pulse lidar observation in Shanghai. *The Science of the Total Environment*, *574*, 1502–1511. https://doi.org/10.1016/j.scitotenv.2016.08.152

Liu, Z., Liu, D., Huang, J., Vaughan, M., Uno, I., Sugimoto, N., et al. (2008). Airborne dust distributions over the Tibetan Plateau and surrounding areas derived from the first year of CALIPSO lidar observations. *Atmospheric Chemistry and Physics*, *8*(16), 5045–5060. https://doi.org/10.5194/acp-8-5045-2008

Lou, M. Y., Guo, J. P., Wang, L. L., Xu, H., Chen, D. D., Miao, Y. C., et al. (2019). On the relationship between aerosol and boundary layer height in summer in China under different thermodynamic conditions. *Earth and Space Science*, *6*(5), 887–901. https://doi.org/10.1029/2019ea000620

Luan, T., Guo, X. L., Guo, L. J., & Zhang, T. H. (2018). Quantifying the relationship between PM2.5 concentration, visibility and planetary boundary layer height for long-lasting haze and fog-haze mixed events in Beijing. *Atmospheric Chemistry and Physics*, *18*(1), 203–225. https://doi.org/10.5194/acp-18-203-2018

Luo, H., Han, Y., Lu, C. S., Yang, J., & Wu, Y. H. (2019). Characteristics of surface solar radiation under different air pollution conditions over Nanjing, China: Observation and simulation. *Advances in Atmospheric Sciences*, *36*(10), 1047–1059. https://doi.org/10.1007/s00376-019-9010-4

Lv, Z., Wei, W., Cheng, S. Y., Han, X. Y., & Wang, X. Q. (2020). Meteorological characteristics within boundary layer and its influence on PM2.5 pollution in six cities of North China based on WRF-Chem. *Atmospheric Environment*, *228*, 117417. https://doi.org/10.1016/j.atmosenv.2020.117417

Malm, W. C., & Day, D. E. (2001). Estimates of aerosol species scattering characteristics as a function of relative humidity. *Atmospheric Environment*, *35*(16), 2845–2860. https://doi.org/10.1016/s1352-2310(01)00077-2

Mao, F. Y., Gong, W., & Li, J. (2012). Geometrical form factor calculation using Monte Carlo integration for lidar. *Optics & Laser Technology*, *44*(4), 907–912. https://doi.org/10.1016/j.optlastec.2011.10.024

Mao, W. S., Wang, Q. Q., Ma, H., & Sheng, G. F. (2008). Temporal and spatial variation characteristics of Meiyu in Jianghuai. *Transactions of Atmospheric Sciences*, *31*(1), 116–122.

Mehta, M., Singh, N., & Anshumali (2018). Global trends of columnar and vertically distributed properties of aerosols with emphasis on dust, polluted dust and smoke - inferences from 10-year long CALIOP observations. *Remote Sensing of Environment*, *208*, 120–132. https://doi.org/10.1016/j.rse.2018.02.017

Menut, L., Flamant, C., Pelon, J., & Flamant, P. H. (1999). Urban boundary-layer height determination from lidar measurements over the Paris area. *Applied Optics*, *38*(6), 945–954. https://doi.org/10.1364/ao.38.000945

Miao, Y. C., Li, J., Miao, S. G., Che, H. Z., Wang, Y. Q., Zhang, X. Y., et al. (2019). Interaction between planetary boundary layer and PM2.5 pollution in megacities in China: A review. *Current Pollution Reports*, *5*(4), 261–271. https://doi.org/10.1007/s40726-019-00124-5

Miao, Y. C., Liu, S. H., Zheng, Y. J., & Wang, S. (2016). Modeling the feedback between aerosol and boundary layer processes: A case study in Beijing, China. *Environmental Science and Pollution Research*, *23*(4), 3342–3357. https://doi.org/10.1007/s11356-015-5562-8

Mona, L., Pappalardo, G., Amodeo, A., D'Amico, G., Madonna, F., Boselli, A., et al. (2009). One year of CNR-IMAA multi-wavelength Raman lidar measurements in coincidence with CALIPSO overpasses: Level 1 products comparison. *Atmospheric Chemistry and Physics*, *9*(18), 7213–7228. https://doi.org/10.5194/acp-9-7213-2009

Oikawa, E., Nakajima, T., & Winker, D. (2018). An evaluation of the shortwave direct aerosol radiative forcing using CALIOP and MODIS observations. *Journal of Geophysical Research: Atmospheres*, *123*(2), 1211–1233. https://doi.org/10.1002/2017jd027247

Omar, A. H., Winker, D. M., Kittaka, C., Vaughan, M. A., Liu, Z. Y., Hu, Y. X., et al. (2009). The CALIPSO automated aerosol classification and lidar ratio selection algorithm. *Journal of Atmospheric and Oceanic Technology*, *26*(10), 1994–2014. https://doi.org/10.1175/2009jtecha1231.1

Pappalardo, G., Wandinger, U., Mona, L., Hiebsch, A., Mattis, I., Amodeo, A., et al. (2010). EARLINET correlative measurements for CALIPSO: First intercomparison results. *Journal of Geophysical Research*, *115*, D00H19. https://doi.org/10.1029/2009jd012147

Petaja, T., Jarvi, L., Kerminen, V. M., Ding, A. J., Sun, J. N., Nie, W., et al. (2016). Enhanced air pollution via aerosol-boundary layer feedback in China. *Scientific Reports*, *6*. https://doi.org/10.1038/srep18998

Proestakis, E., Amiridis, V., Marinou, E., Georgoulias, A. K., Solomos, S., Kazadzis, S., et al. (2018). Nine-year spatial and temporal evolution of desert dust aerosols over South and East Asia as revealed by CALIOP. *Atmospheric Chemistry and Physics*, *18*(2), 1337–1362. https://doi.org/10.5194/acp-18-1337-2018

Qu, Y. W., Han, Y., Wu, Y. H., Gao, P., & Wang, T. J. (2017). Study of PBLH and its correlation with particulate matter from one-year observation over Nanjing, Southeast China. *Remote Sensing*, *9*(7), 14. https://doi.org/10.3390/rs9070668

Quan, J. N., Tie, X. X., Zhang, Q., Liu, Q., Li, X., Gao, Y., & Zhao, D. L. (2014). Characteristics of heavy aerosol pollution during the 2012-2013 winter in Beijing, China. *Atmospheric Environment*, *88*, 83–89. https://doi.org/10.1016/j.atmosenv.2014.01.058

Redemann, J., Vaughan, M. A., Zhang, Q., Shinozuka, Y., Russell, P. B., Livingston, J. M., et al. (2012). The comparison of MODIS-Aqua (C5) and CALIOP (V2 & V3) aerosol optical depth. *Atmospheric Chemistry and Physics*, *12*(6), 3025–3043. https://doi.org/10.5194/acp-12-3025-2012

Sawyer, V., & Li, Z. Q. (2013). Detection, variations and intercomparison of the planetary boundary layer depth from radiosonde, lidar and infrared spectrometer. *Atmospheric Environment*, *79*, 518–528. https://doi.org/10.1016/j.atmosenv.2013.07.019

Seinfeld, J. H., & Pandis, S. N. (2012). *Atmospheric chemistry and physics: From air pollution to climate change*. Wiley.

Shao, P., Xin, J. Y., An, J. L., Kong, L. B., Wang, B. Y., Wang, J. X., et al. (2017). The empirical relationship between PM2.5 and AOD in Nanjing of the Yangtze River Delta. *Atmospheric Pollution Research*, *8*(2), 233–243. https://doi.org/10.1016/j.apr.2016.09.001

Shen, J., & Cao, N. W. (2020). Comprehensive observation and analysis of aerosol optical properties and vertical distribution in Nanjing, China. *Atmospheric Environment*, *239*. https://doi.org/10.1016/j.atmosenv.2020.117767

Solanki, R., & Singh, N. (2014). LiDAR observations of the vertical distribution of aerosols in free troposphere: Comparison with CALIPSO level-2 data over the central Himalayas. *Atmospheric Environment*, *99*, 227–238. https://doi.org/10.1016/j.atmosenv.2014.09.083

Stull, R. B. (1988). *An introduction to boundary layer meteorology* (pp. 680). Kluwer Academic Publishers. https://doi.org/10.1007/978-94-009-3027-8

Su, T. N., Li, Z. Q., & Kahn, R. (2018). Relationships between the planetary boundary layer height and surface pollutants derived from lidar observations over China: Regional pattern and influencing factors. *Atmospheric Chemistry and Physics*, *18*(21), 15921–15935. https://doi.org/10.5194/acp-18-15921-2018

Su, T. N., Li, Z. Q., Li, C. C., Li, J., Han, W. C., Shen, C. Y., et al. (2020). The significant impact of aerosol vertical structure on lower atmosphere stability and its critical role in aerosol-planetary boundary layer (PBL) interactions. *Atmospheric Chemistry and Physics*, *20*(6), 3713–3724. https://doi.org/10.5194/acp-20-3713-2020

Sun, J., Zhang, L., Shen, X., Che, H., Zhang, Y., Fan, R., et al. (2016). A review of the effects of relative humidity on aerosol scattering properties. *Acta Meteorologica Sinica*, *74*(5), 672–682.

Sun, T. Z., Che, H. Z., Qi, B., Wang, Y. Q., Dong, Y. S., Xia, X. G., et al. (2019). Characterization of vertical distribution and radiative forcing of ambient aerosol over the Yangtze River Delta during 2013-2015. *The Science of the Total Environment*, *650*, 1846–1857. https://doi.org/10.1016/j.scitotenv.2018.09.262

Sun, W., Liu, Z., Videen, G., Fu, Q., Muinonen, K., Winker, D. M., et al. (2013). For the depolarization of linearly polarized light by smoke particles. *Journal of Quantitative Spectroscopy & Radiative Transfer*, *122*, 233–237. https://doi.org/10.1016/j.jqsrt.2012.03.031

Tan, I., Storelvmo, T., & Choi, Y. S. (2014). Spaceborne lidar observations of the ice-nucleating potential of dust, polluted dust, and smoke aerosols in mixed-phase clouds. *Journal of Geophysical Research: Atmospheres*, *119*(11), 6653–6665. https://doi.org/10.1002/2013jd021333

Tsang, T. T., Pai, P., & Korgaonkar, N. V. (1988). Effect of temperature, atmospheric condition, and particle size on extinction in a plume of volatile aerosol dispersed in the atmospheric surface layer. *Applied Optics*, *27*(3), 593–598. https://doi.org/10.1364/ao.27.000593

Twomey, S. (1977). The influence of pollution on the shortwave albedo of clouds. *Journal of the Atmospheric Sciences*, *34*(7), 1149–1152. https://doi.org/10.1175/1520-0469(1977)034<1149:tiopot>2.0.co;2

Twomey, S. A., Piepgrass, M., & Wolfe, T. L. (1984). An assessment of the impact of pollution on global cloud albedo. *Tellus Series B: Chemical and Physical Meteorology*, *36B*(5), 356–366. https://doi.org/10.3402/tellusb.v36i5.14916

Tyagi, S., Tiwari, S., Mishra, A., Singh, S., Hopke, P. K., Singh, S., & Attri, S. D. (2017). Characteristics of absorbing aerosols during winter foggy period over the national capital region of Delhi: Impact of planetary boundary layer dynamics and solar radiation flux. *Atmospheric Research*, *188*, 1–10. https://doi.org/10.1016/j.atmosres.2017.01.001

Uno, I., Sugimoto, N., Shimizu, A., Yumimoto, K., Hara, Y., & Wang, Z. F. (2014). Record heavy PM2.5 air pollution over China in January 2013: Vertical and horizontal dimensions. *Sola*, *10*, 136–140. https://doi.org/10.2151/sola.2014-028

Wang, L. Y., Lyu, B. L., & Bai, Y. Q. (2020). Aerosol vertical profile variations with seasons, air mass movements and local PM2.5 levels in three large China cities. *Atmospheric Environment*, *224*, 11. https://doi.org/10.1016/j.atmosenv.2020.117329

Wang, W., Gong, W., Mao, F. Y., & Pan, Z. X. (2016). An improved iterative fitting method to estimate nocturnal residual layer height. *Atmosphere*, *7*(8). https://doi.org/10.3390/atmos7080106

Winker, D. M., Hunt, W. H., & McGill, M. J. (2007). Initial performance assessment of CALIOP. *Geophysical Research Letters*, *34*(19), L19803. https://doi.org/10.1029/2007gl030135

Winker, D. M., Tackett, J. L., Getzewich, B. J., Liu, Z., Vaughan, M. A., & Rogers, R. R. (2013). The global 3-D distribution of tropospheric aerosols as characterized by CALIOP. *Atmospheric Chemistry and Physics*, *13*(6), 3345–3361. https://doi.org/10.5194/acp-13-3345-2013

Wong, M. S., Qin, K., Lian, H., Campbell, J. R., Lee, K. H., & Sheng, S. J. (2017). Continuous ground-based aerosol Lidar observation during seasonal pollution events at Wuxi, China. *Atmospheric Environment*, *154*, 189–199. https://doi.org/10.1016/j.atmosenv.2017.01.051

Wu, Y., Cordero, L., Gross, B., Moshary, F., & Ahmed, S. (2014). Assessment of CALIPSO attenuated backscatter and aerosol retrievals with a combined ground-based multi-wavelength lidar and sunphotometer measurement. *Atmospheric Environment*, *84*, 44–53. https://doi.org/10.1016/j.atmosenv.2013.11.016

Yang, Q., Yuan, Q., Yue, L., Li, T., Shen, H., & Zhang, L. (2019). The relationships between PM2.5 and aerosol optical depth (AOD) in mainland China: About and behind the spatio-temporal variations. *Environmental Pollution*, *248*, 526–535. https://doi.org/10.1016/j.envpol.2019.02.071

Yang, X., Zhao, C. F., Guo, J. P., & Wang, Y. (2016). Intensification of aerosol pollution associated with its feedback with surface solar radiation and winds in Beijing. *Journal of Geophysical Research: Atmospheres*, *121*(8), 4093–4099. https://doi.org/10.1002/2015jd024645

Yang, Y., Chan, C.-y., Tao, J., Lin, M., Engling, G., Zhang, Z., et al. (2012). Observation of elevated fungal tracers due to biomass burning in the Sichuan Basin at Chengdu city, China. *The Science of the Total Environment*, *431*, 68–77. https://doi.org/10.1016/j.scitotenv.2012.05.033

Ye, X. X., Song, Y., Cai, X. H., & Zhang, H. S. (2016). Study on the synoptic flow patterns and boundary layer process of the severe haze events over the North China Plain in January 2013. *Atmospheric Environment*, *124*, 129–145. https://doi.org/10.1016/j.atmosenv.2015.06.011

Yu, H. B., Chin, M., Winker, D. M., Omar, A. H., Liu, Z. Y., Kittaka, C., & Diehl, T. (2010). Global view of aerosol vertical distributions from CALIPSO lidar measurements and GOCART simulations: Regional and seasonal variations. *Journal of Geophysical Research*, *115*, D00H30. https://doi.org/10.1029/2009jd013364

Zhang, T., Che, H. Z., Gong, Z. Q., Wang, Y. Q., Wang, J. Z., Yang, Y. Q., et al. (2020). The two-way feedback effect between aerosol pollution and planetary boundary layer structure on the explosive rise of PM2.5 after the "Ten Statements of Atmosphere" in Beijing. *The Science of the Total Environment*, *709*, 9. https://doi.org/10.1016/j.scitotenv.2019.136259

Zheng, C. W., Zhao, C. F., Zhu, Y. N., Wang, Y., Shi, X. Q., Wu, X. L., et al. (2017). Analysis of influential factors for the relationship between PM2.5 and AOD in Beijing. *Atmospheric Chemistry and Physics*, *17*(21), 13473–13489. https://doi.org/10.5194/acp-17-13473-2017

Zhu, J., Xia, X. G., Che, H. Z., Wang, J., Cong, Z. Y., Zhao, T. L., et al. (2019). Spatiotemporal variation of aerosol and potential long-range transport impact over the Tibetan Plateau, China. *Atmospheric Chemistry and Physics*, *19*(23), 14637–14656. https://doi.org/10.5194/acp-19-14637-2019

Zilitinkevich, S. S., Tyuryakov, S. A., Troitskaya, Y. I., & Mareev, E. A. (2012). Theoretical models of the height of the atmospheric boundary layer and turbulent entrainment at its upper boundary. *Izvestiya, Atmospheric and Oceanic Physics*, *48*(1), 133–142. https://doi.org/10.1134/s0001433812010148